



An investigation on the energy absorption capability of aluminum foam-filled multi-cell tubes

Mehmet Ali Güler¹ · Sinem K. Mert² · Murat Altin³ · Erdem Acar⁴

Received: 26 May 2023 / Accepted: 21 August 2023 / Published online: 25 September 2023
© The Author(s), under exclusive licence to The Brazilian Society of Mechanical Sciences and Engineering 2023

Abstract

Aluminum foams are employed more and more in the automobile sector in order to increase the crashworthiness of energy absorbers. This study examines the energy absorption potential of multi-cellular tubes filled with Al foams. The mean crush forces of foam-filled tubes are calculated using a theoretical model that takes into account the effects of the tube, the foam, and their interaction. A numerical model including the damage constitutive equations is also built to examine the additional crashworthiness properties, such as specific energy absorption and crush force efficiency. The numerical and theoretical models are validated through experiments under quasi-static axial loading, where crashworthiness metrics and deformation images of the tubes are compared. It is observed that the inclusion of damage criteria in the numerical simulation can accurately simulate the deformation of the tubular specimens. It was discovered that foam-filled tubes efficiently absorbed more energy without considerably adding to their total weight compared to hollow, thin-walled tubes. Inserting aluminum foam inside the T4 multi-cell tube improved energy absorption (EA) and crush force efficiency (CFE) by 140 and 84%, respectively. Similarly, inserting aluminum foam inside the T8 multi-cell tube improved EA and CFE by 60 and 34%, respectively. It is also found that the mean force values of empty and foam-filled multi-cell tubes can be predicted using an empirical formula with an error less than 5 and 15%, respectively. Due to their high stiffness-to-weight ratio and energy absorption capacity, foam-filled multi-cell tubes can be utilized as energy absorbers to reduce damage and additional harm to the passengers in the event of an accident.

Keywords Crashworthiness · Energy absorption · Ls-Dyna · Theoretical model · Al 6061 multi-cell tubes · Al foam

Technical Editor: João Marciano Laredo dos Reis.

✉ Mehmet Ali Güler
mehmet.guler@aum.edu.kw

Sinem K. Mert
sinemkocaoglanmert@gmail.com

Murat Altin
maltin@gazi.edu.tr

Erdem Acar
acar@etu.edu.tr

¹ College of Engineering and Technology, American University of the Middle East, Egaila 54200, Kuwait

² Department of Mechanical Engineering, Ankara Yildirim Beyazit University, Ankara 06010, Turkey

³ Department of Automotive Engineering, Gazi University, Ankara 06500, Turkey

⁴ Department of Mechanical Engineering, TOBB University of Economics and Technology, Ankara 06560, Turkey

1 Introduction

Crashworthiness of a vehicle can be defined as the potential of its structure to safeguard the occupants by absorbing the energy in the case of an accident. Within the last couple of decades, the studies on the crashworthiness of structures have been carried out to improve the energy absorption capability of the structures. In order to absorb more energy, multi-cell tubes having several different sections such as square, triangular, and hexagonal were studied. Nia and Parsapour [1] tested simple and multi-cell thin-walled aluminum tubes with square, triangular, octagonal, and hexagonal geometries to quasi-static loads. The research revealed that multi-cell tubes have a higher energy absorption capability than alternative designs. The multi-cell tubes with hexagonal and octagonal shapes absorbed the highest energy per mass. Fang et al. [2] examined the crashworthiness of square multi-cell tubes with various cell numbers under both axial and oblique loads. They found that, the number of cells has a

positive effect on the energy absorption (EA) but a negative effect on the peak force of multi-cell tubes. Tang et al. [3] examined the effect of the geometrical properties of square and cylindrical multi-cell tubes on the energy absorption capabilities and discovered that the circular multi-cell tubes performed better than the square counterparts. Similarly, Zhang and Zhang [4] investigated the geometric effects on the energy absorption characteristics of axially compressed circular multi-cell tubes having single, double, triple, and quadruple cell sections. They observed that the specific energy absorption (SEA) of quadruple multi-cell columns are 30% higher than the other sections studied. Yang and Feng [5] modeled a star-shaped multicellular tube in Abaqus. According to their study, the star-shaped quadrangular multicellular tube (SSMT-4-14) has a crush force efficiency that is 1.24 times greater than that of the star-shaped quadrangular tube (SST-4-14) for the same wall thickness conditions. For the same mass, SSMT-4-14 has an energy absorption that is 1.17 times greater than that of SST-4-14 and a crush force efficiency that is 1.14 times greater than that of SST-4-14. Koloushani et al. [6] investigated the impact of thickness on the thin-walled circular tube. According to the research, increasing thickness enhances CFE, and rising the thickness to diameter (t/D) ratio enhances SEA and CFE. Ma and Tian [7] proposed a new hybrid multi-cell structure that includes both round and diamond shapes. They discovered that the hybrid order of the multi-cell structure significantly affects the mechanical properties and increases energy absorption, enhancing crashworthiness. Albak et al. [8] examined the crashing behaviors of seven distinct graphene-inspired multi-cell tubes under different loading angles (0, 10, 20, and 30 degrees). Their work demonstrated that adding hollow cylinders to multi-cell tubes made of graphene improved crashworthiness. Under axial loading, the structures with second-order hollow cylinders showed a more stable form of deformation. Attar et al. [9] investigated the effect of adding stiffeners to the outer tube wall and the multi-cell effect of the structure. According to their results, the SEA and CFE was increased up to 89% and 52%, respectively, in comparison with the reference tube by placing stiffeners in the middle sides of the tube wall and building a multi-cell tube. Wu et al. [10] studied the energy absorption capacity of the multi-cell structures subjected to impact conditions. To compare the multi-cell tubes with various cross-sectional configurations, they considered three representative topological configurations. Their findings demonstrated that the number of cells in multi-cell tubes can increase MCF and

SEA. They concluded that, when compared to alternative sectional configurations of the same mass, the five-cell tube exhibits the greatest crashworthiness characteristics. Chen et al. [11] proposed four thin-walled hybrid multi-cell structures with circular and square sections. The tube's size and the structure's wall thickness affected energy absorption. They discovered that the hybrid multi-cell tube with an inner square portion and a circle on the outside performed the best in terms of crashworthiness.

Recently multi-cell tubes with aluminum foam filling attracted many researchers to study their energy absorption performance since it has a lower density compared to other metal foams. A foam-filled elliptical tube was investigated by Gao et al. [12] under various loading angles, and they compared the elliptical tubes with other hollow and foam-filled tubes, such as square, circular, and rectangular tubes. They observed that foam-filled elliptical tubes had higher SEA than the other tubes. A similar study was conducted by Kılıçaslan [13] on corrugated circular tubes that were both empty and filled with aluminum foam. Their study indicated that the double-tube designs with aluminum foam filling had higher SEA than others. Qi and Yang [14] and Ahmad and Thambiratnam [15] compared the foam-filled and empty thin-walled conical tubes and showed the benefits of foam-filled conical tubes used as energy absorbers. Although the initial peak force was unaffected by the foam density, the overall amount of energy absorbed increased as the density increased. Toksoy and Guden [16] investigated both filled and empty commercial 1050H14 Al tubes with Alulight foam under quasi-static conditions. The SEA and mean load were increased when the tubes were partially filled with foam. Similarly, Altin et al. [17] investigated the ability of circular and square tubes and several foam filling ratios under quasi-static loading. According to their results, the SEA of a square design with foam filling was five times greater than that of a square design without foam. By changing the wall thickness, the CFE and SEA values of the foam-filled square designs were enhanced by 42% and 87%, respectively. Nikkhah et al. [18] and Zhang and Cheng [19] modeled foam-filled aluminum 6060 tubes. Nikkhah et al. [18] showed that simple tubes absorbed more energy than windowed tubes for the majority of load angles, although circular and square windowed tubes absorbed more energy than other windowed tubes. Zhang and Cheng [19] minimized the first peak force and enhanced the energy absorption of multi-cell tubes by employing a pre-crushed trigger. Li et al. [20] designed multi-cell circumferentially

Table 1 Foam properties used in numerical analyses [61]

σ_f (g/cm ³)	σ_p (GPa)	α	α_2	β	γ (GPa)	ϵ_D
0.628	0.0325	2.12	2.1273	9.6	0.0175	1.4584

corrugated square tubes to enhance the crushing performance of conventional multi-cell tubes. The multi-corrugation designs were made by applying a cosine expression to the cross section of tubes. According to their results, the mean force of the circumferentially corrugated square tubes with multiple cells increased exponentially as the number of cells and corrugations increased.

Few numerical studies on the energy absorption performance of thin-walled structures under static and dynamic conditions include damage criteria. Reyes et al. [21] and Qiao et al. [22] examined square thin-walled columns using a damage model with geometric defects in the FE model. Marzbanrad et al. [23] investigated the collapse of a circular tube made of the extruded aluminum alloy EN AW-7108 T6 using a ductile failure criterion. In the studies of Allahbakhsh et al. [24] and Estrada et al. [25, 26], FE models for an aluminum alloy were developed based on Hooputra's ductile damage model [27]. Aforementioned studies used ductile, shear, and damage initiation criteria in addition to the Müschenborn-Sonne Forming Limit Diagram (MSFLD). Moreover, Estrada et al. [28] concentrated on the modeling of progressive damage in bi-tubular aluminum 6063-T5 structures with square, circular, and polygonal cross-sections as well as circular discontinuities. The bitubular structures were modeled by applying the Johnson-Cook (J-C) failure theory. Mert et al. [29] investigated the crashworthiness performance of thin-walled multi-cell tubes under quasi-static conditions. Johnson Cook damage model was used to model the deformation of tubes in ABAQUS. When compared to shell elements, solid elements were shown to be more successful in simulating the crush behavior of thin-walled aluminum tubes. When shell elements were used, the deformation pattern was inaccurate due to the nodes at the top of the thin-walled tube's rotating degree of freedom during the initial contact with the rigid upper plate. Therefore, with the model which includes shell elements, an unrealistic folding was obtained. However, when the solid elements were employed in the simulations rather than the shell elements, a better prediction of folding at the center of the tube was produced. Additionally, the initial peak load was greatly influenced by the element number in the thickness direction.

Several different material models have been used to describe the deformation behavior of foams. A visco-elastic-plastic foam material model (LAW 33) in RADIOSS, simple model with geometric boundaries with MAT_SOIL_AND_FOAM (MAT_005), a nonlinear elastoplastic material model with MAT_HONEYCOMB (MAT_26), crushable foam model with optional damping and tension cutoff with MAT_CRUSHABLE_FOAM (MAT_063), and isotropic crushable foam model with MAT_BILKHU/DUBOIS_FOAM (MAT_075) in LS-DYNA were used to simulate metallic foams. Under impact loading, Goel [30] compared the empty and foam-filled circular and square tubes and

found that foam-filled circular tubes absorbed more energy than square ones. He used visco-elastic-plastic foam material model (LAW 33 in RADIOSS) in modeling the aluminum foams. Different material models, including MAT_5, MAT_26, MAT_63, and MAT_75, were used to simulate metallic foams in LS-DYNA. Hanssen et al. [31] found that these material models were unable to capture changes in foam density and compressibility that occur during deformation. Additionally, these models cannot be improved to incorporate the change in compressibility. The self-similar evolution model and differential hardening model were proposed by Deshpande and Fleck [32]. Reyes et al. [33] implemented the foam model of Deshpande and Fleck with the self-similar evolution model determining the initial yield surface's shape. They were able to accurately predict the material behavior using a stress-based fracture criterion. Using MAT_154 (MAT_DESHPANDE_FLECK_FOAM) material model for aluminum foam, Altun et al. [17] and Zhang and Cheng [19] accurately predicted the collapse mechanism of aluminum tubes filled with foam. They discovered that square tubes filled with foam had the optimum energy absorption capabilities. Aforementioned investigations all agreed that placing metallic foam inside the tubes increased their energy absorption capacity. Yin et al. [34] studied foam-filled aluminum 6060 multi-cell thin-walled structures with various number of cells. They examined multi-cell square tubes with various cell numbers which were filled with aluminum foam. According to their numerical results, the multi-cell tubes with nine cells provides the best crashworthiness performance. Zhang et al. [35] investigated the benefits of several filling styles on the crashworthiness of aluminum 6060 multi-cell square structures, including honeycomb filling, foam filling, and compound filling of honeycomb and foam. The elastic linear strain-hardening model MAT_24 in LS-DYNA is used to model the tube walls and honeycomb shells. Their results showed that the multi-cell square tube's corner cells performed best in terms of crashworthiness when honeycombs were used to partially fill them. The best results are obtained when two diagonally opposed corner cells are filled with foam. Sun et al. [36] used the piecewise linear plasticity material model, MAT_24, in LS-DYNA to study the impacts of cross-sectional configurations and foam-filler in the aluminum 6060 multi-cell tubes. In comparison with different topological configurations, their results demonstrated that the five-cell tube with four corner cells filled with foams was the best energy absorber.

Theoretical studies were also conducted for estimating the crashworthiness behavior of empty and foam-filled single-cell metallic tubes. Alexander [37] conducted an analytical study on prediction of the collapse load of empty cylinders performing as energy absorbers. Abramowicz and Wierzbicki studied the crushing mechanics of empty columns

with right angle corners [38] and later columns with corners having arbitrary angle [39]. The main outcome of both studies was obtaining a theoretical equation for the mean crush force in terms of material and geometrical parameters. [40] also investigated the dynamic axial crushing of empty square tubes and also both static and dynamic crushing of circular and square tubes experimentally and theoretically by including inertial effects [41]. Andrews et al. [42] did an experimental study on the quasi-static compression of empty Al alloy tubes for prediction of the mean crush load and classification of collapse modes. Santosa and Wierzbicki [43] did a theoretical study on the quasi-static axial crushing of tubes with low-density filler material, such as aluminum foam or honeycomb. They discovered that aluminum foam was less weight-efficient than honeycomb filling. Hanssen et al. [44] investigated the effects of foam density and wall thickness on the deformation behavior of aluminum foam-filled circular tubes under quasi-static and dynamic loads. Santosa et al. [45] derived an expression for the mean crush force prediction of the steel tubes filled with aluminum foam based on experiments. The mean crush force of the filled tube was dependent on the foam strength and the tube shape. Chen and Wierzbicki [46] simplified the formula of Wierzbicki and Abramowicz [38] and introduced the Simplified Super Folding Element (SSFE) Theory to predict the mean force of simple and multi-cell tubes filled with foams. The overall crushing resistance was found to be raised by 80% of the direct foam resistance due to the interaction between the foam and the tube wall. Niknejad et al. [47, 48] investigated the crushing force and absorbed energy of square tubes filled with polyurethane foam experimentally and theoretically taking the interaction of the tube wall and polyurethane foam into account. Similarly, the crush force and absorbed energy of empty and polyurethane foam-filled rectangular and square tubes were calculated by Abedi et al. [49]. They calculated the instantaneous folding force, which depends on the tube's wall thickness, edge length, and flow stress of the tube material. Sun et al. [50] theoretically investigated the folding mechanism of empty and foam-filled, single and multi-cell aluminum square tubes with functionally graded thicknesses.

There are a quite a few theoretical studies on the empty and foam-filled multi-cell tubes. The mean force of empty multi-cell square tubes was derived by Xie et al. [51] and Zhang et al. [52]. The tapered multi-cell tubes filled with foam were studied by Googarchin et al. [53] to compute the mean force by superposing the mean forces of the empty tube, the foam filler, and their interactions.

Reyes et al. [21] examined quasi-static tests of square AA6060 columns and modeled the tubes with LS-DYNA utilizing the MAT-103 material model to predict energy absorbing capacity. Applying the anisotropic plasticity model resulted in good accuracy for estimating peak load when compared to mean load. Square tubes exhibited buckling deformation mode, and energy absorption was reduced as loading angles were increased. Marzbanrad et al. [23] examined the crash behavior of aluminum alloy circular tubes using Abaqus for numerical analysis. To produce reliable crashworthiness simulation results, the ductile failure criterion along with elastic and plastic boundary conditions were used on the bottom of the tube. According to their findings, using an elastic boundary altered the mode of deformation and reduced the peak force. Estrada et al. [25] examined the impact of discontinuities on the crashworthiness performance of aluminum 7108 tubes using Abaqus. In the discrete models, the shear, ductile, and M \ddot{u} sch \ddot{u} born-Sonne Forming Limit Diagram (MSFLD) damage initiation criteria were used to take into account the ductile material properties of aluminum alloys. Adding discontinuities resulted in a peak force reduction of up to 4.74% compared to a tube without holes and an increase of 7% and 12.69% in energy absorption and crush force efficiency, respectively. Later, Estrada et al. [26] used these criteria to investigate the aluminum 7108 concentric and multi-cell tubes. The tubes with circular cross-section showed the best performance. Qiao et al. [22] modeled 6063 aluminum alloy as an elastoplastic material in Abaqus. They used the shear failure damage model for the crack initiation and evolution. Their concluded that the material microstructure, impact speed, boundary conditions, and geometrical dimensions affected the crashworthiness of aluminum tube. Googarchin et al. [53] simulated the energy absorption process of Al1060 tubes with Al foam filler using

Table 2 Analysis Results of multi-cell empty T4E Model

	Peak force (kN)	Mean force (kN)	CFE	EA (kJ)	Mass (kg)	SEA (kJ/kg)
T4E1	259.87	102.56	0.39	9.230	0.447	20.649
T4E2	259.87	97.98	0.38	8.818	0.446	19.771
T4E3	251.20	99.94	0.40	8.995	0.436	20.630
T4E Ave.	256.98	100.16	0.39	9.014	0.443	20.350
FEA	269.88	93.98	0.35	8.458	0.452	18.712
Error (%)	5.02	-6.17	-10.26	-6.17	2.03	-8.05

Table 3 Analysis Results of multi-cell empty T8E Model

	Peak force (kN)	Mean force (kN)	CFE	EA (kJ)	Mass (kg)	SEA (kJ/kg)
T8E1	246.41	108.16	0.44	9.734	0.435	22.377
T8E2	238.04	112.28	0.47	10.105	0.431	23.446
T8E3	240.45	89.27	0.37	8.034	0.429	18.727
T8E Ave.	241.63	103.24	0.43	9.291	0.432	21.507
FEA	269.55	93.68	0.35	8.431	0.452	18.653
Error (%)	11.55	-9.26	-18.60	-9.26	4.63	-13.27

Table 4 Comparison of mean force predicted by FE model and formula for multi-cell empty tubes

Geometry	Mean force (kN)	Simulation result (kN)	Error (%)	Empirical formula (kN)	Error (%)
T4E	100.16	93.98	-6.17	104.81	4.64
T8E	103.24	93.68	-9.26	101.68	-1.51

Abaqus. Elastic-plastic-damage and elastic-strain softening-densification model assumptions were used to describe the mechanical behavior of Al1060 and Al foam, respectively. The forming limit diagram and the stress-strain curve for the elastic-plastic property of Al1060 were used as criteria for the damage initiation. Moreover, the effective plastic displacement theory for Al 1060 was used to define linear damage progression.

Despite numerous numerical investigations that employs a damage model to predict the axial crushing behavior of empty and foam-filled single-cell tubes, to the best of authors’ knowledge, there is no numerical study in the literature that employed a damage model to predict axial crushing of empty and foam-filled multi-cell tubes. Therefore, it is vital to develop a numerical model capable of predicting the progressive as well as catastrophic failure mechanisms of empty and foam-filled multi-cell tubes. In this study, developed numerical model is accompanied with theoretical and experimental studies to validate its performance on aluminum multi-cell foam-filled tubes.

The paper is organized as follows: Sect. 2 discusses the theoretical models for predicting mean crush force of empty and foam-filled tubes. Section 3 presents the details of the numerical model (finite element model) developed in this study. Experimental study is discussed in Sect. 4. The results obtained for empty and foam-filled tubes are presented in Sect. 5. Conclusions derived from this study are given in Sect. 6.

2 Theoretical model

Wierzbicki and Abramowicz [38] developed a theoretical model to investigate the mean force of a square tube. Using a Super Folding Element (SFE), they were able to forecast the mean force of the square and rectangular columns, while taking the extensional and bending modes into account using the formula:

$$P_m = 9.56\sigma_0 b^{\frac{1}{3}} t^{\frac{5}{3}} \tag{1}$$

where P_m is the mean force t and b are thickness and the width of the tube and σ_0 is the flow stress of the material.

Similarly, Zhang et al. [52] calculated the mean crush force of empty square multi-cell tubes subdivided into equal cells using the following formula:

$$P_m = \sigma_0 t \sqrt{(4N_C + 2N_T + N_O)} \pi L_c t \tag{2}$$

where N_T is number of T shapes, N_C is number of criss-cross sections, and N_O is number of corners.

Based on the study of Abramowicz and Wierzbicki [38], Xie et al. [51] estimated the mean force of empty multi-cell tubes using the energy balance equation.

$$P_m 2Hk = E_{\text{Bending}} + E_{\text{Membrane}} \tag{3}$$

where $2H$ is height of a superfolding element, k is the effective crush distance coefficient, E_{Bending} is the bending energy and E_{Membrane} is the membrane energy due to plastic deformation. The formula for mean force is given by Xie et al. [51] as

$$P_m = \frac{1}{2k} \sigma_0 t \sqrt{(4N_T + 2N_L + 3.65N_I + 8N_C + 5.4N_{II})} \pi L_c t \tag{4}$$

where σ_0 is the flow stress of the material, t is the wall thickness, and L_c is the total length of all flanges. Moreover, N_T is number of T shapes, N_L is number of left corners, N_I is number of 3 panel type I, N_C is number of criss-crosses and N_{II} is number of 3 panel type II elements of the structure as shown in Fig. 1.

Table 5 Analysis results of multi-cell foam-filled T4FF Model

	Peak force (kN)	Mean force (kN)	CFE	EA (kJ)	Mass (kg)	SEA (kJ/kg)
T4FF1	349.70	204.99	0.59	18.449	1.010	18.266
T4FF2	328.10	274.40	0.84	24.696	1.156	21.363
T4FF3	333.0	244.03	0.73	21.963	1.036	21.200
T4FF Ave.	336.93	241.14	0.72	21.703	1.067	20.340
FEA	355.74	236.17	0.66	21.255	1.035	20.536
Error (%)	5.58	-2.06	-8.33	-2.06	-3.00	0.96

Table 6 Analysis Results of multi-cell foam-filled T8FF Model

	Peak force (kN)	Mean force (kN)	CFE	EA (kJ)	Mass (kg)	SEA (kJ/kg)
T8FF1	336.80	165.94	0.49	13.275	0.987	13.450
T8FF2	315.70	221.67	0.70	17.735	1.046	16.955
T8FF3	310.0	172.71	0.56	13.817	1.038	13.311
T8FF Ave.	320.83	186.78	0.58	14.942	1.024	14.592
FEA	321.52	218.72	0.68	17.498	1.035	16.906
Error (%)	0.21	17.10	17.24	17.11	1.07	15.86

The flow stress of the material is calculated from:

$$\sigma_0 = \sqrt{\frac{\sigma_y \sigma_u}{1 + n}} \tag{5}$$

where σ_y is the yield stress, σ_u is the ultimate stress and n is the strain hardening exponent.

Following the aforementioned studies on empty tubes, Gogarchin et al. [53] proposed a theoretical mean crush force formula for the foam-filled tubes by combining the mean forces of the empty tube, the foam filler, and their interactions, as depicted in Fig. 2.

They formulated the mean force as:

$$P_m = P_{\text{tube}} + P_{\text{foam}} + P_{\text{interaction}} \tag{6}$$

where P_{tube} is calculated from Eq. (5), P_{foam} and $P_{\text{interaction}}$ can be calculated from [53].

$$P_{\text{foam}} = \sigma_f A_f \tag{7}$$

$$P_{\text{interaction}} = C_{\text{avg}} \sqrt{\sigma_f \sigma_0} ct \tag{8}$$

$$c = \frac{a + b}{2} \tag{9}$$

where σ_0 is the flow stress of the material, A_f is the area of foam, σ_f is the plateau stress, t is the wall thickness, a and b are the foam cross-section and C_{avg} is a nondimensional

Table 7 Comparison of mean force predicted by FE model and formula for multi-cell foam filled tubes

Geometry	Mean force (kN)	Simulation result (kN)	Error (%)	Empirical formula (kN)	Error (%)
T4FF	241.14	236.17	-2.06	204.82	-13.0
T8FF	186.78	218.72	17.10	208.69	11.73

constant and equal to 5.5 [53]. Therefore mean force of the foam-filled tube can be calculated as:

$$P_m = P_{\text{tube}} + \sigma_f A_f + C_{\text{avg}} \sqrt{\sigma_f \sigma_0} ct \tag{10}$$

In this section, mean crush force was estimated using the formulas presented above. However, in order to understand the overall crashworthiness characteristics of the foam-filled tubes it is necessary to develop a numerical model which will be described in the next section.

3 Finite element modeling

3.1 Construction of the FEA model

Ls-Dyna is used to model the deformation process which includes splitting and tearing of the aluminum tubes. Two different multi-cell tube configurations were designed and

Table 8 Comparison of CFE and SEA for multi-cell empty and foam-filled tubes (experimental results)

Model	CFE	SEA (kJ/kg)
T4E Ave	0.39	20.35
T8E Ave	0.43	21.51
T4FF Ave	0.72	20.34
T8FF Ave	0.58	14.59

labeled as T4E and T8E based on the number of rectangular space in the cross section as shown in Fig. 3. Multi-cell tube T4E was designed by locating square tubes to the corners of a single-cell tube and then dividing the cross-section into four. Multi-cell tube T8E was designed by locating rectangular tubes to the corners of a single-cell tube and then dividing the remaining portion into four.

Fully integrated shell elements with five integration points are used to simulate aluminum tubes. In the simulations, the aluminum tubes are discretized with shell elements using Belytcko-Tsay formulation, and foam is modeled using constant stress solid elements. For hourglass control standard LS-DYNA viscous form is applied which is default option. In the FE model, platens are modeled as

rigid plates using MAT_20_RIGID material model as displayed in Fig. 4. The upper rigid plate was allowed to move only along the height of the tube, and the lower one was constrained from all degrees of freedom.

In order to deform the tubes over the fixed plate, the moving plate is given a downward velocity of 2 mm/ms in the FE analysis. Velocity is ramped up to the final value within a specific amount of time similar to the study of Acar et al. [54]. During the first 50 ms of our FE study, the moving plate’s velocity is scaled up from 0 to 2 mm/ms.

3.2 Material models used in this study

3.2.1 Material model for the Al tube

The material model of the aluminum tube is described by MAT_18 (MAT_POWER_LAW_PLASTICITY) [55].

In MAT_18, the aluminum tube is modeled with an isotropic plasticity model with rate effects which uses a power law hardening rule. However, this material model can also be used for strain rate independent materials such as Al alloys ([56–59]) by not activating the strain rate parameters by setting SRC=SRP=0 in the model.

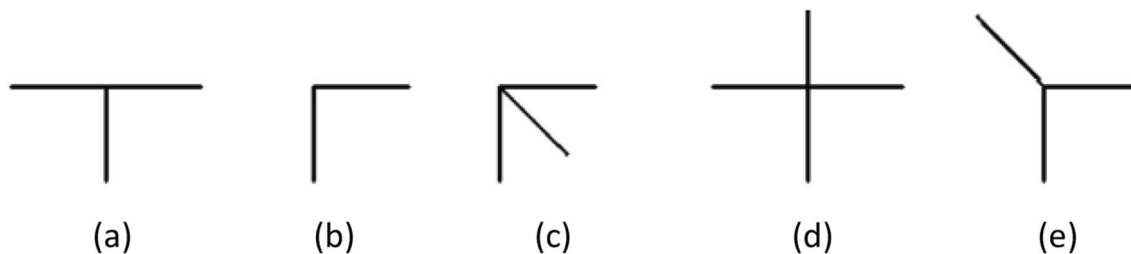
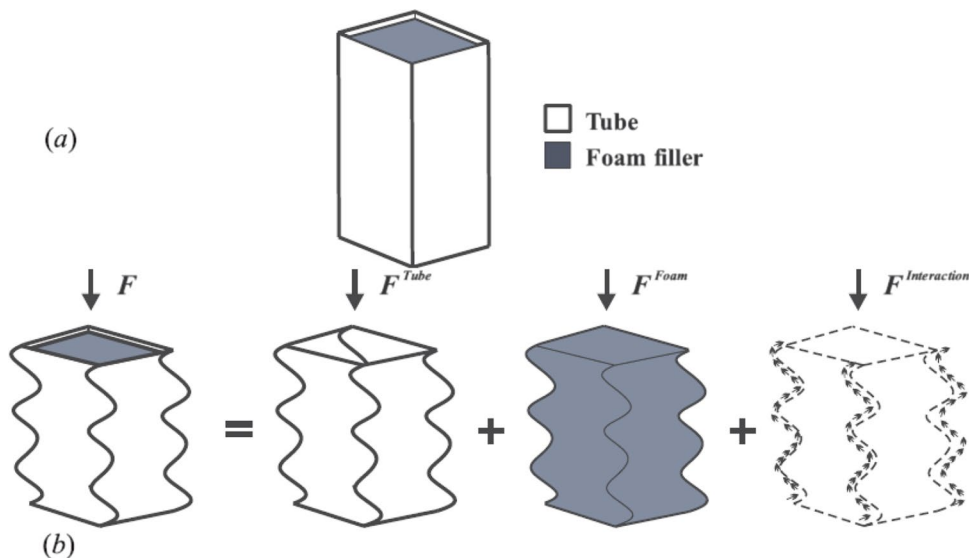


Fig. 1 Corner Elements of Structures **a** T shape **b** left corner **c** 3 panel type **d** criss-cross **e** 3 panel type II [51]

Fig. 2 Figure 2. Mean Force Calculation Mechanism **a** a foam-filled tube **b** mean crush loads due to the empty tube P_{tube} , the foam-filler P_{foam} , and the interaction effect $P_{interaction}$ [53]



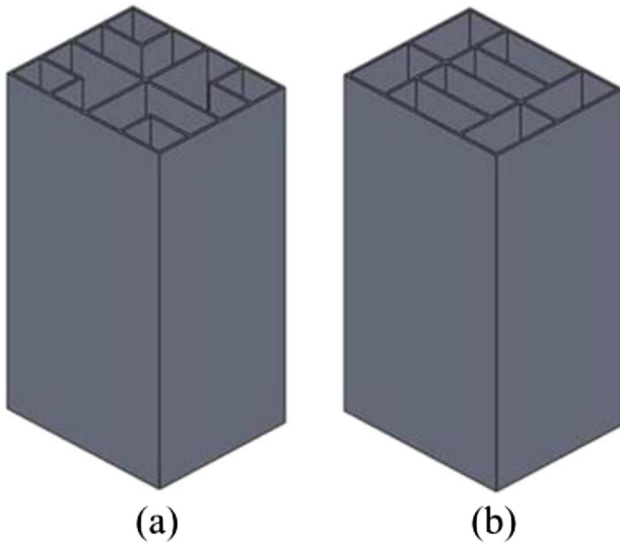


Fig. 3 Geometry of the multi-cell empty tubes **a** Tube T4E **b** Tube T8E

The yield stress σ_y , which depends on plastic strain, is calculated using the equation:

$$\sigma_y = k\epsilon^n = k(\epsilon_{yp} + \bar{\epsilon}^p)^n \tag{11}$$

where k is strength coefficient, ϵ_{yp} is the elastic strain to yield and $\bar{\epsilon}^p$ is the effective plastic strain. If σ_y is set to zero, the strain to yield can be calculated by finding the point where the strain hardening equation (Eq. (11)) and the linearly elastic loading equation ($\sigma_y = E\epsilon$) intersect. Then, the elastic strain at yield can be found as:

$$\epsilon_{yp} = \left(\frac{E}{k}\right)^{\frac{1}{n-1}} \tag{12}$$

If σ_y is nonzero and greater than 0.02 then the elastic strain at yield becomes

$$\epsilon_{yp} = \left(\frac{\sigma_y}{k}\right)^{\frac{1}{n}} \tag{13}$$

In this study, the rectangular tube is made of Al 6061-T6 with the following elastic properties: material density is 2700 kg/m^3 , Young's modulus is 68.9 GPa; Poisson's ratio is 0.33, strength coefficient is 0.3788, hardening exponent is 0.050692 [60].

In MAT_18, element deletion occurs when the plastic failure strain in the model is exceed. The tears at the corners of the tube are observed when the plastic failure strain is exceed. The plastic failure strain for element deletion is set to 0.48 based on a parametric study that provides consistent results compared to the experiments.

3.2.2 Material model for the Al foam

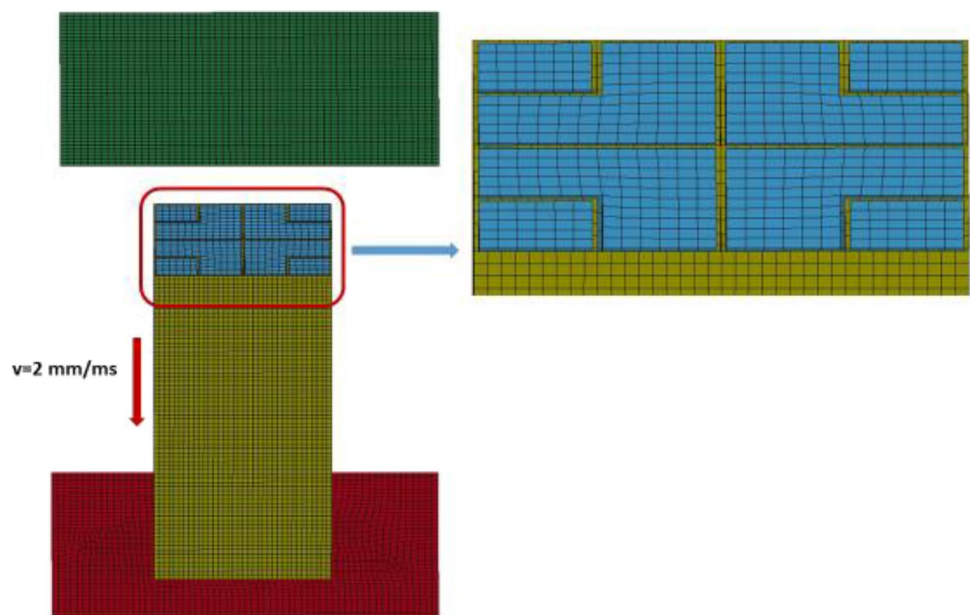
In this study Aluminum alloy foam (AlMg1Si0.6TiH20.8) with a density of 0.628 g/cm^3 was placed inside the tubes. The material for the metallic foam made of aluminum is defined by MAT_154 (MAT_DESPANDE_FLECK_FOAM) [55].

According to the yield criterion, the aluminum foam is modeled with:

$$\phi = \hat{\sigma} - \sigma_y \leq 0 \tag{14}$$

where ϕ is the yield stress function, σ_y is the yield stress, and the equivalent stress $\hat{\sigma}$ is calculated from:

Fig. 4 Finite element model of aluminum multi-cell empty T4E tube



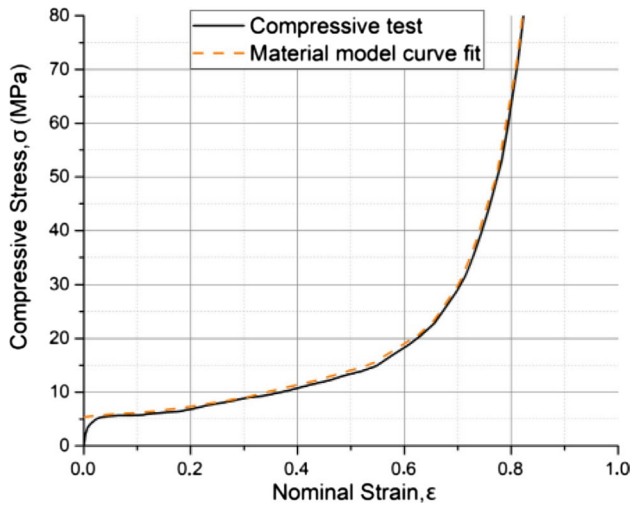


Fig. 5 Stress–strain curve for the Al foam used in FEA models [61]

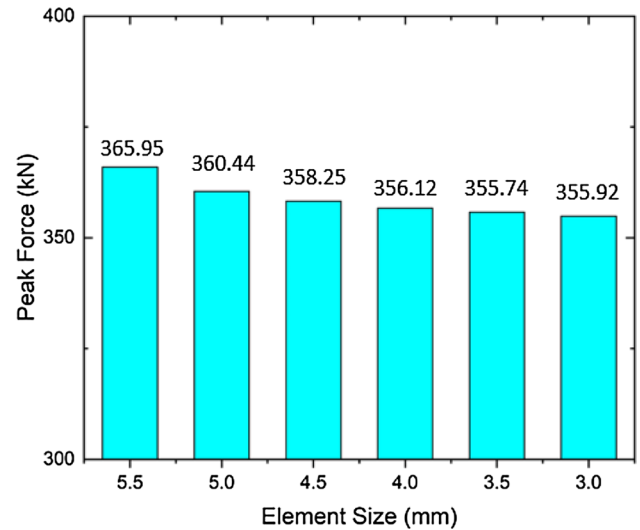


Fig. 7 Mesh convergence study for multi-cell foam-filled T4FF tube

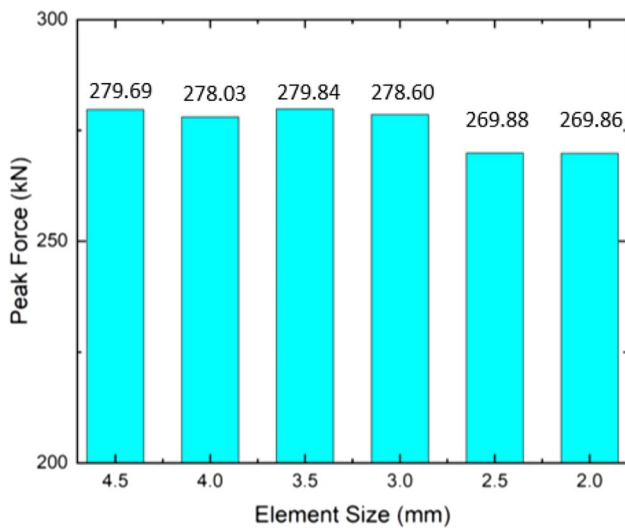


Fig. 6 Mesh convergence study for multi-cell empty T4E tube

$$\hat{\sigma} = \sqrt{\frac{1}{1 + \left(\frac{\alpha}{3}\right)^2}} (\sigma_e^2 + \alpha^2 \sigma_m^2) \tag{15}$$

where σ_m is the mean stress and σ_e is the von Mises effective stress, respectively. The parameter α is used to calculate the yield surface and α is calculated as [61]:

$$\alpha^2 = \frac{9(1 - 2\vartheta^p)}{2(1 + \vartheta^p)} \tag{16}$$

where ϑ^p is the plastic coefficient of contraction. For the foam, ϑ^p is equal to zero [61], then the material parameter α can be computed as 2.12 from Eq. (18). The yield stress can then be expressed as follows [61]:

$$\sigma_y = \sigma_p + \gamma \frac{\hat{\epsilon}}{\epsilon_D} + \alpha_2 \ln \left(\frac{1}{1 - \left(\frac{\hat{\epsilon}}{\epsilon_D}\right)^\beta} \right) \tag{17}$$

where σ_p is the plateau stress, $\hat{\epsilon}$ is the equivalent strain and γ , α_2 and β are hardening parameters. The densification strain (compaction strain) is determined as [61]

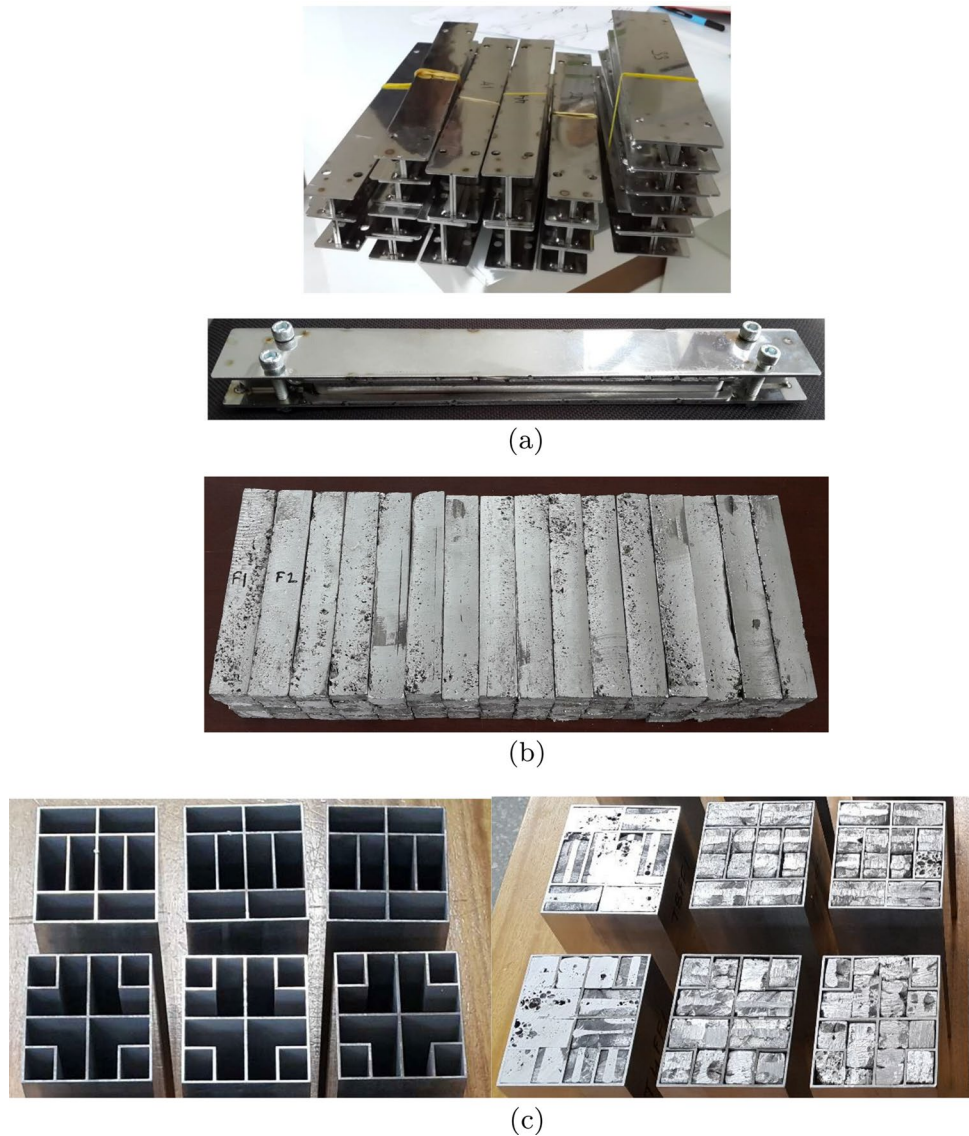
$$\epsilon_D = -\frac{9 + \alpha^2}{3\alpha^2} \ln \left(\frac{\rho_f}{\rho_0} \right) \tag{18}$$

where ρ_f is the foam density, and ρ_0 is the density of the virgin material. The material parameters used in Eqs. (17),(18) are given in Table 1 [61]. By fitting the test data as shown in Fig. 5, the empirical constants that constitute the foam model’s parameters can be determined. In our earlier study [61], we minimized the discrepancy between the mathematical material model and the test data using a particle swarm optimization algorithm in MATLAB software.

3.3 Contact definitions

In the FEA model, the lower rigid wall is restricted from all degrees of freedom while the upper rigid plate is only permitted to move along the length of the tube. Using the AUTOMATIC_SINGLE_SURFACE_CONTACT algorithm, the tube’s self-contact is represented. The AUTOMATIC_SURFACE_TO_SURFACE_CONTACT algorithm is used to represent the interaction between the tube and plates. The AUTOMATIC_SURFACE_TO_SURFACE_CONTACT algorithm is also employed for the foam-filled tubes to model the interaction between the tube and the aluminum foam. Soft constraint formulation (SOFT=1)

Fig. 8 Test specimens for all configurations: **a** Molds used to prepare Al foams **b** Al foams prepared using the molds **c** Empty and foam-filled test specimens



is selected in the contact card for the model of foam-filled tubes. The static and dynamic friction coefficients are taken as 0.3 and 0.2, respectively, as used in our previous studies [17, 54, 61, 62].

3.4 Mesh convergence study

The convergence of the FEA model of the tube is investigated by varying the element size between 2 to 3.5 mm in discretization of the multi-cell T4E tube. Figure 6 depicts the predicted peak forces of T4E multi-cell tubes for various element sizes. According to Fig. 6, an element size of 2.5 mm is acceptable in terms of accuracy and computational cost.

The convergence of the FEA model of the foam is explored by varying the element size between 3 to 4.5 mm in discretization of the foam. Figure 7 shows the predicted peak forces of multi-cell T4FF tubes for various element

sizes. According to Fig. 7, an element size of 3.5 mm is sufficient in terms of accuracy and computational cost.

4 Experimental study

The empty and foam-filled versions of the rectangular tubes are used in the experiments as shown in Fig. 8. The aluminum foam was produced in molds as shown in Figure 8a. The produced foam (see Fig. 8b) are then inserted to the empty tubes to obtain the foam filled tubes as shown in Fig. 8c.

The tubes have a length of 180 mm, a wall thickness of 1.5 mm, and a cross-section of 71.5 mm × 86.5 mm. To minimize the manufacturing costs, rectangular tubes are manufactured using wire erosion method. This method is a fast and practical method for prototype production phase

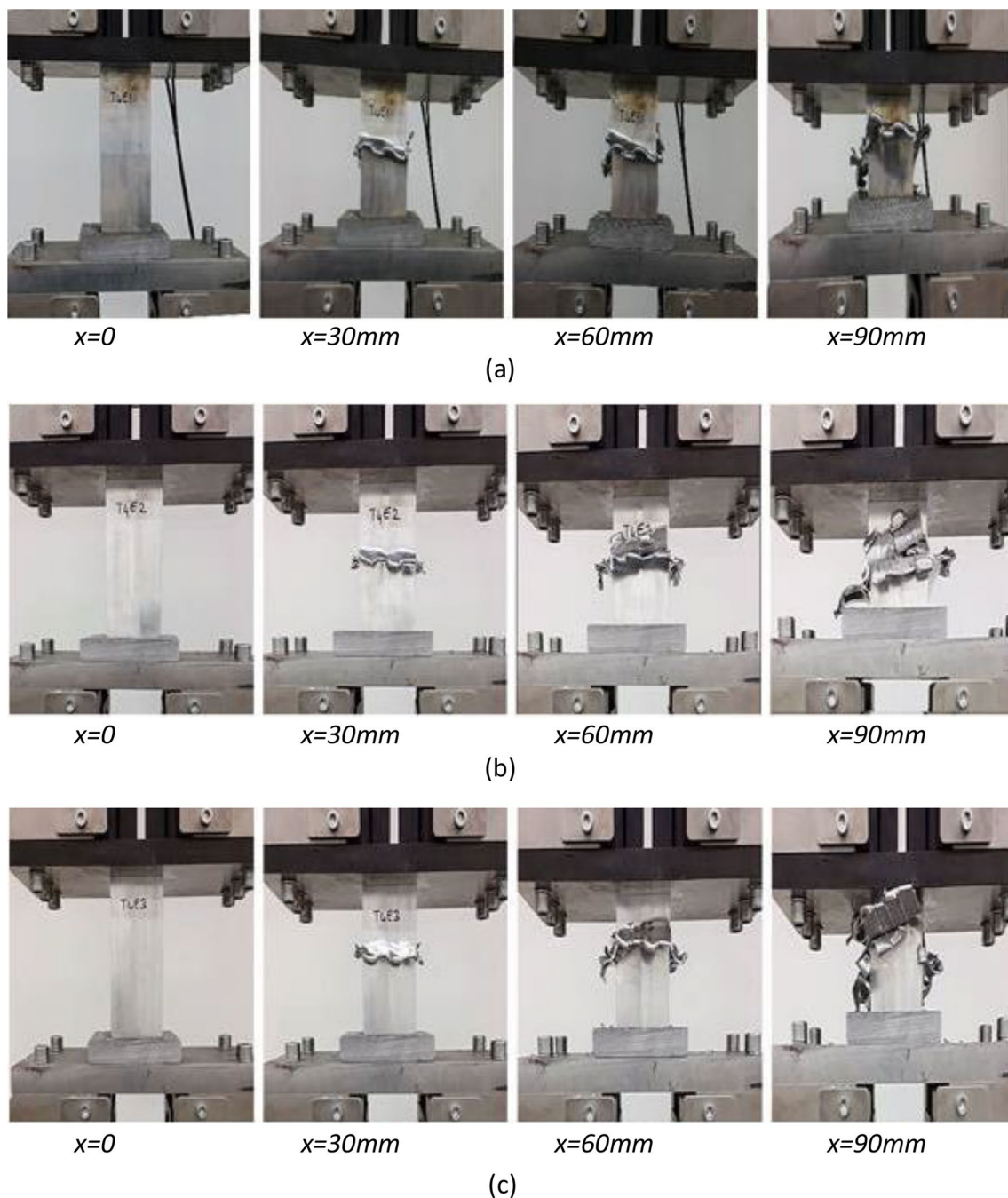


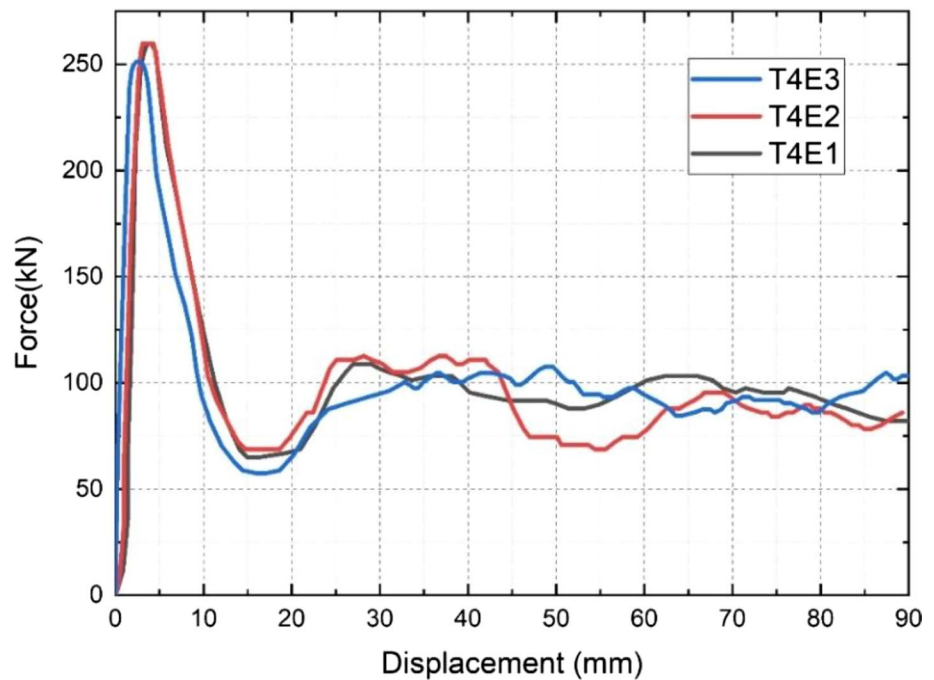
Fig. 9 Deformation views of multi-cell empty T4E test specimens at different displacements: $x = 0$ mm, $x = 30$ mm, $x = 60$ mm, $x = 90$ mm a T4E1 b T4E2 c T4E3

for limited number of products but it is not suitable for mass production in terms of both time and cost. Due to the sharp corners of the tubes, tearing and crack formation are observed at the corners during the experiments. The excessive stresses at the corners due to stress concentration and the application of high temperatures during the wire erosion method caused the tube corner parts to deteriorate their load carrying capacity.

4.1 Axial crushing experiments of the empty T4E multi-cell tubes

The rigid plate moves downward with a speed of 2 mm/min during experiments. Tubes are deformed until their half-length (90 mm). The identical tests were computed on three specimens with the same geometry to verify the repeatability

Fig. 10 Force-displacement graph of multi-cell empty T4E test specimens



of the experiments. The deformation images of the T4E tubes until 90 mm of deformation are given in Fig. 9.

The deformation in T4E tubes started in the middle and cracks started to occur before 30 mm of displacement of the upper rigid plate. The force-displacement figures obtained from the experiments of empty multi-cell T4E tubes are given in Fig. 10.

The peak crush force occurs around 250 kN in T4E tubes. After reaching the peak value, the crush force decreases to a minimum value around 70 kN and then increases up to around 110 kN. It is observed that the tubes did not deform in a progressive manner rather they teared from the corners in the middle of the tubes. Then, the crush force fluctuates between 70 kN and 110 kN until the end of the deformation. By using the force-displacement graphs in Fig. 10, the energy absorption parameters of the T4E tubes can be calculated.

4.2 Axial crushing experiments of the empty T8E multi-cell tubes

The deformed images of the T8E tubes within 90 mm of deformation are given in Fig. 11. As in the case of T4E tubes, cracks formed in the middle region of T8E multi-cell tubes, after a deformation distance of approximately 20 mm. Due to these cracks, tearing starts in the middle of the tubes. Figure 12 shows that the peak crush force is around 250 kN as in the case of T4E multi-cell tubes following a dip at

around 70 kN. Afterwards crush force fluctuates between 70 kN and 125 kN until the end of the deformation.

4.3 Axial crushing experiments of the foam-filled T4FF multi-cell tubes

The test conditions remain the same for foam filled tubes. The deformation images obtained within a compression distance of 90 mm for foam-filled T4 multi-cell tubes, named as T4FF, are given in Fig. 13. The force-displacement graphs obtained from the experiments of T4FF tubes are given in Fig. 14. The average peak crush force is around 325 kN in T4FF tubes. After this value, the crush force decreases to 175 kN. The deformation behavior of foam-filled tubes is different than the empty tubes. The tearing starts near the ends of the tubes in foam-filled tubes rather than the middle of the tubes observed in empty tubes.

4.4 Axial crushing experiments of the foam-filled T8FF multi-cell tubes

Figure 15 depicts the deformation images of foam-filled T8 multi-cell tubes (T8FF). As can be seen from the pictures, T8FF multi-cell tubes start to tear from the ends of the tubes as in the case of the T4FF tubes. The force-displacement graphs for T8FF tubes are given in Fig. 16. The test was terminated for specimen 1 when the deformation distance was 80 mm since the tube T8FF1 entirely collapsed.

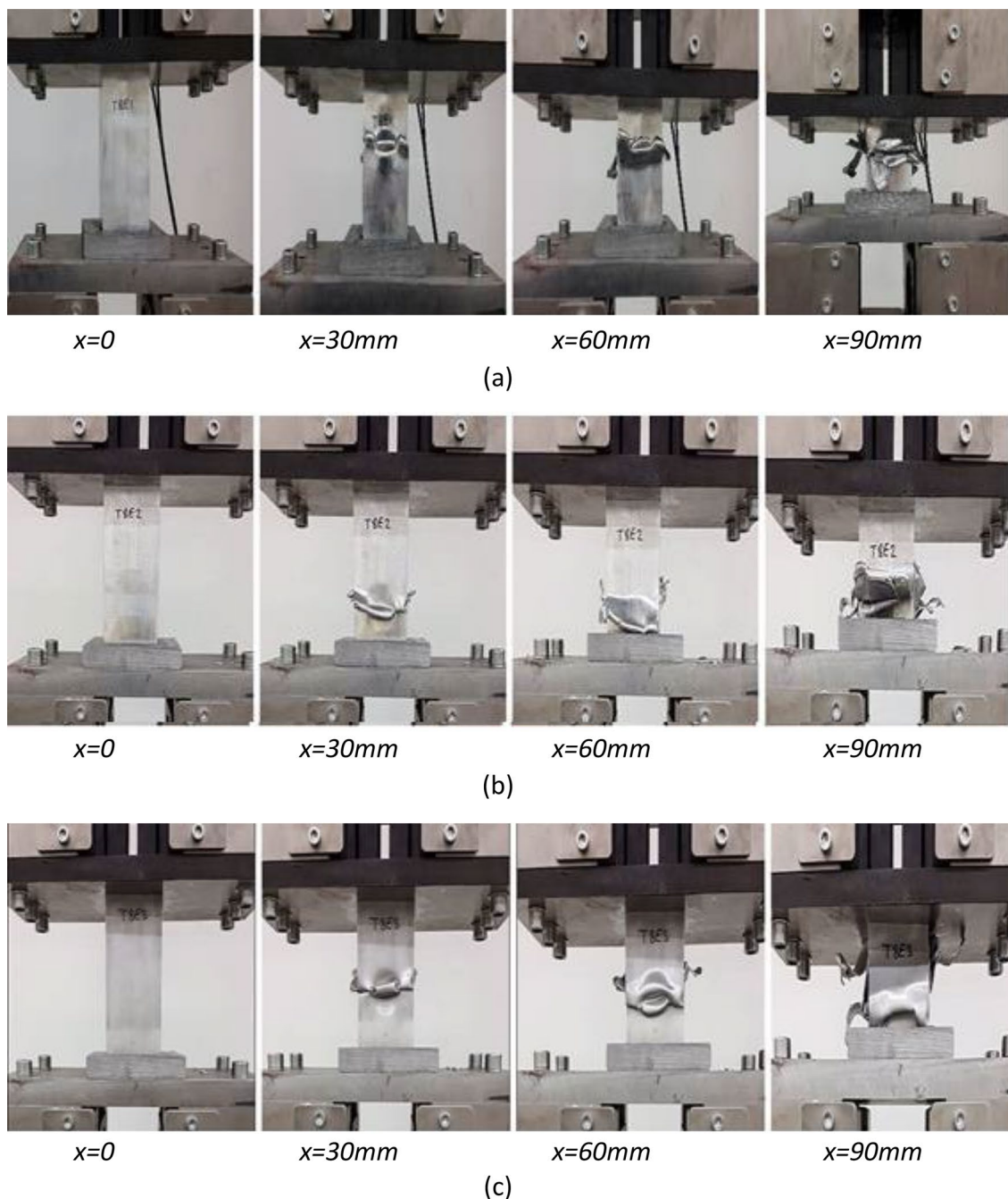


Fig. 11 Deformation views of multi-cell empty T8E specimens at different displacements: $x = 0$ mm, $x = 30$ mm, $x = 60$ mm, $x = 90$ mm **a** T8E1 **b** T8E2 **c** T8E3

5 Results and discussion

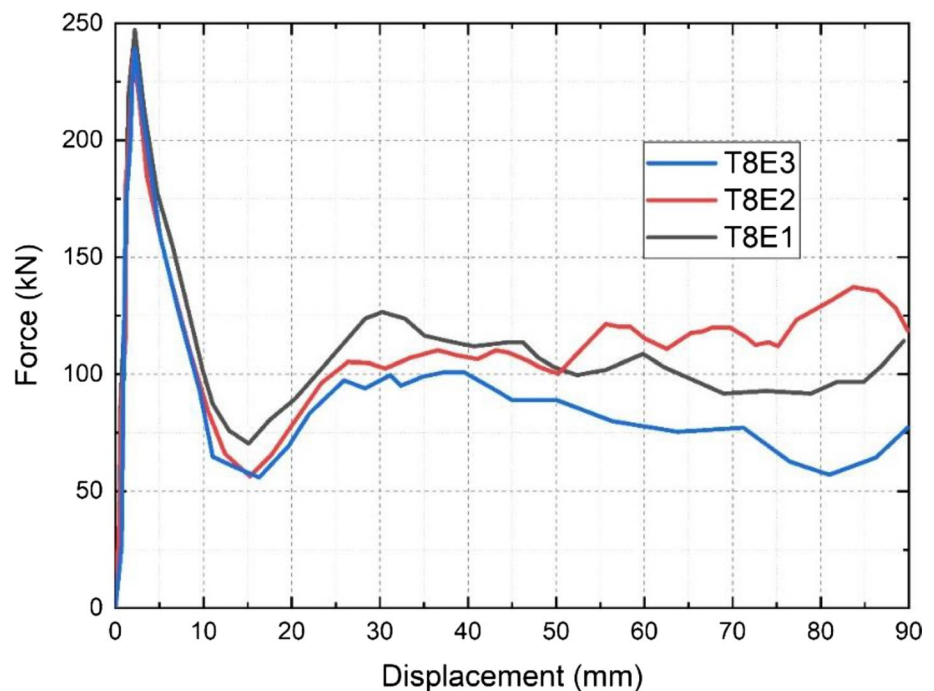
5.1 Empty tubes

5.1.1 Experimental and FEA results for empty T4E multi-cell tubes

Figure 17 shows the load–displacement curves for T4E multi-cell tubes obtained from the tests and the FE model.

The comparison of the deformed view of the empty rectangular tubes observed during experiments and obtained through the numerical model are shown in Fig. 18. As can be seen in Fig. 17, deformations start to occur in the tubes when the compression load reaches the level of approximately 250 kN. However, the crack formation at mid height of the tube reduces the crash force after peak force is observed. Failure of the tubes is observed to be in tearing mode and crack formation causes force fluctuation between 50 kN and 115

Fig. 12 Force-displacement graph of multi-cell empty T8E test specimens



kN. After the deformation begins, splitting and tearing of the tubes are seen at the specimens' midpoint in both experiments and the FE model (see Fig. 18). It is observed that the cracks on the tube cause the tubes to rupture and fail catastrophically to the upper side of the tube after 60 mm of deformation.

The crashworthiness metrics for T4E multi-cell tubes are listed in Table 2. The average EA of test specimens is calculated to be 9.014 kJ, whereas the corresponding EA value obtained through FEA is 8.458 kJ with a -6.17% error. The average SEA of test specimens is found to be 20.350 kJ/kg. FEA results for SEA are within 8.05% error as compared to the experimental results. The maximum error between the experimental and FEA results is in CFE value which is 10.26%.

5.1.2 Experimental and FEA results for empty T8E multi-cell tubes

Figure 19 compares the force-displacement graphs of T8E multi-cell tubes derived from the experiments and the FE model. Force-displacement graph for T8E shows similar behavior as compared to the force-displacement graph for T4E. When Figs. 17 and 19 are compared, it is observed that T8E shows wider range of oscillations after 20 mm of deformation (between 60 and 140 kN). Failure starts in the form of crack and fold formation at the corners of the tube near the lower end of the tube as shown in Fig. 20. A catastrophic failure develops to the lower end of the tube after 60 mm of

deformation. The numerical model successfully captures the fracture that occurs at the folded region's corners.

Crashworthiness metrics for the T8E multi-cell tubes are presented in Table 3. The average EA of T8E specimens is calculated to be 9.291 kJ, whereas the corresponding EA value obtained through FEA is 8.431 kJ with a -9.26% error. The average SEA of test specimens is found to be 21.507 kJ/kg. FEA results for SEA are within 13.27% error as compared to the experimental results. The maximum error between the experimental and FEA results is in CFE value which is 18.60%. When the crashworthiness characteristics are examined, it is discovered that the FEA model is in good agreement with the test findings for both T4E and T8E tubes.

5.1.3 Theoretical results for empty T4E and T8E multi-cell tubes

The material properties for aluminum 6061 T6 tubes are obtained from literature [63, 64]. The ultimate strength, σ_u and the yield strength, σ_y are 310.0 MPa and 276 MPa, respectively [63]. The hardening exponent, n is 0.05 [64]. The flow stress, σ_0 can be calculated from Eq. (5) as 285.5 MPa.

Mean crush force can be calculated using Eq. (4) where the effective crush distance of multi-cell tubes, k is assumed to be equal to 0.65 for aluminum 6061 multi-cell tubes [53]. For the tube T4E, the following parameters are used in Eq. (4): $L_c = 316$ mm, $N_T = 12$, $N_C = 1$, $N_L = 8$ and $t = 1.5$ mm. Therefore, the mean crush force for T4E is found to be $P_m = 104.8$ kN.

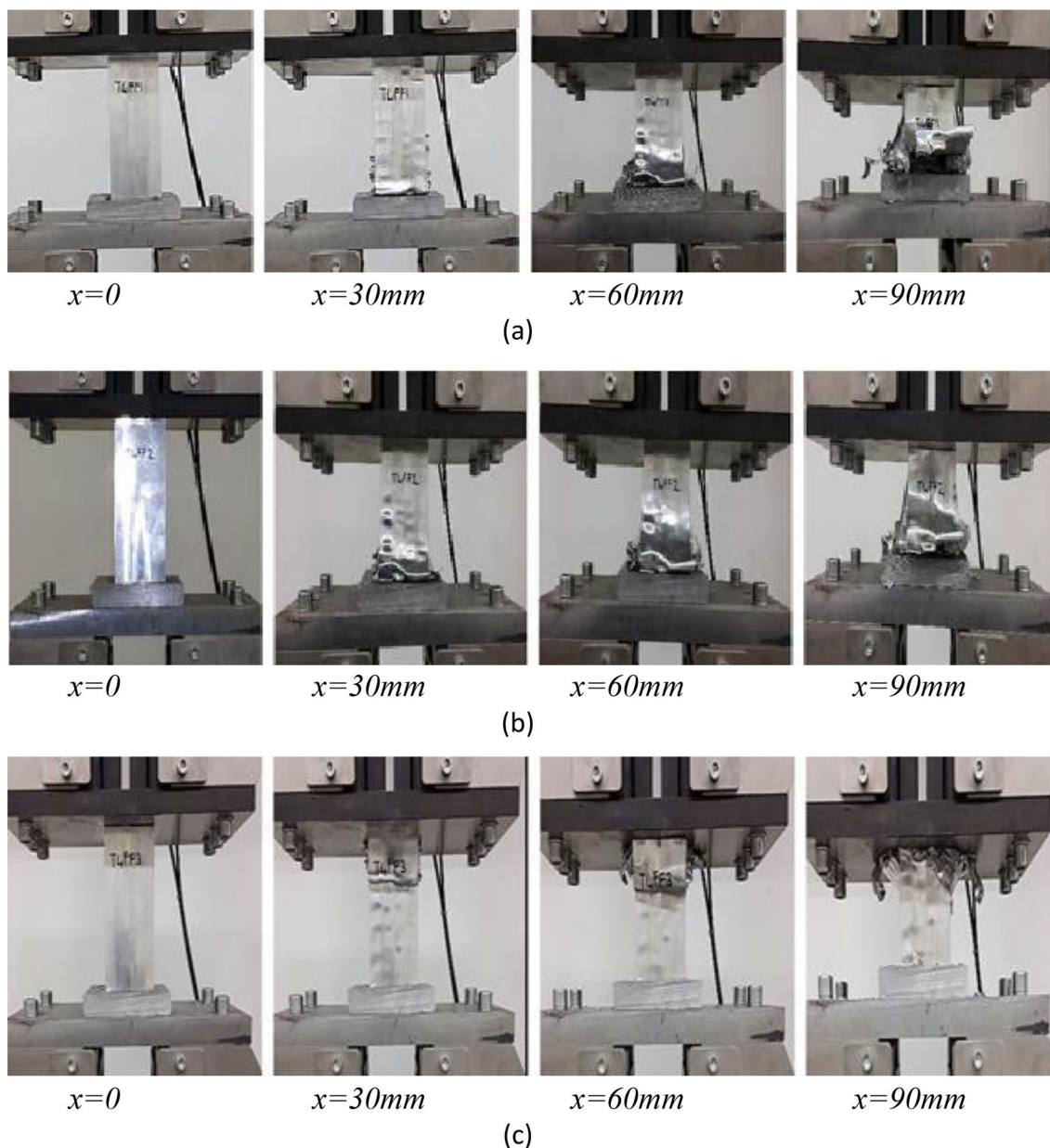


Fig. 13 Deformation views of multi-cell foam-filled T4FF specimens at different displacements: $x = 0$ mm, $x = 30$ mm, $x = 60$ mm, $x = 90$ mm
a T4FF1 **b** T4FF2 **c** T4FF3

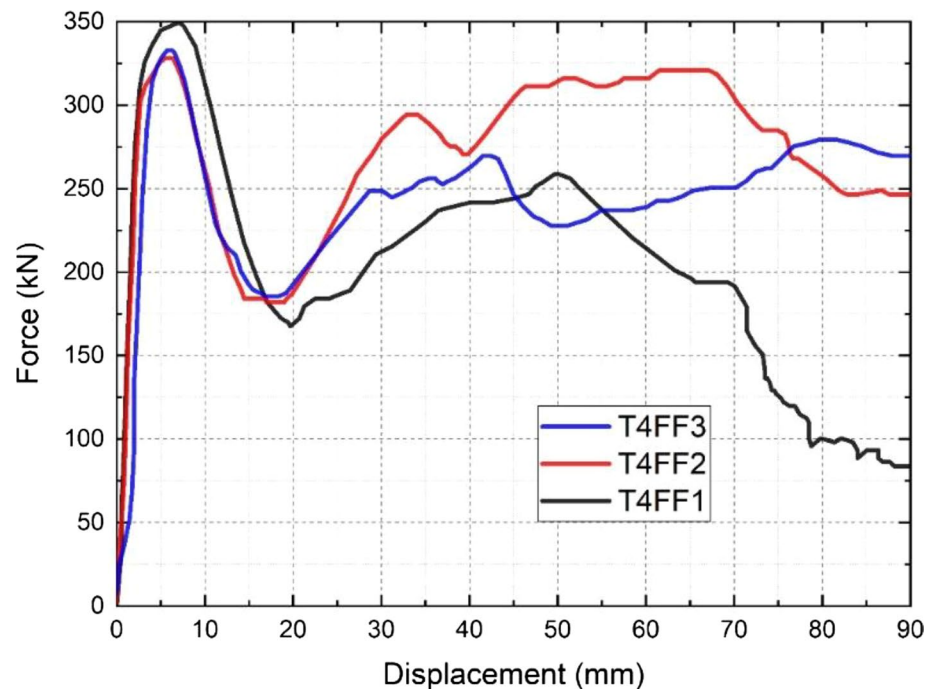
For the tube T8E; $L_c=316$ mm, $N_T=10$, $N_C=2$, $N_L=4$ and $t = 1.5$ mm. Using Eq. (4), the mean crush force for T4E is found to be $P_m = 101.7$ kN.

Calculated mean forces are 104.8 kN and 101.7 kN for T4E and T8E multi-cell tubes, respectively. Table 4 displays the mean crush force that the simulation and empirical formula predict.

The mean force according to empirical formula is 104.8 kN, with a 4.64% error, as compared to the mean force

obtained via tests, which is 100.2 kN for T4E tubes. The mean force according to the empirical formula is 101.7 kN for T8E tubes, with a -1.51% error, as compared to the mean force obtained via tests, which is 103.2 kN for T4E tubes. The simulation values coincide with the mean forces derived from the empirical formula and experimental results.

Fig. 14 Force-displacement graph of multi-cell foam-filled T4FF test specimens



5.2 Foam-filled tubes

5.2.1 Experimental and FEA results for foam-filled T4FF multi-cell tubes

Similar to the empty tubes, foam-filled multi-cell tubes T4FF and T8FF are modeled in Ls-Dyna with the same contact algorithms and material tube properties. Figure 21 compares the force-displacement graphs for T4FF multi-cell tubes obtained from the tests and the FEA model. The deformed images of the experimental and FEA results are compared in Fig. 22. Figure 21 shows that the peak force occurs around 325 kN, which is an indication of the first fold or crack formation. Tearing of the tube near the mid-height is observed at approximately 30 mm of deformation, with a catastrophic failure at the upper part of the tube at 90 mm of deformation (see Fig. 22). Multi-cell T4FF tubes do not show progressive deformation in both experiments and FE predictions.

Crashworthiness metrics for the T4FF multi-cell tubes are presented in Table 5. The average SEA of T4FF specimens is calculated to be 20.340 kJ/kg, whereas the corresponding SEA value obtained through FEA is 20.536 kJ/kg, with a 0.96% error. The maximum error between the experimental and FEA results is in CFE value which is 8.33%. Table 5 shows that the crashworthiness metrics obtained from the FEA model is in good agreement with the test results.

5.2.2 Experimental and FEA results for foam-filled T8FF multi-cell tubes

Figure 23 compares the force-displacement graphs of T8FF multicell tubes obtained from the tests and the FEA model. The images of the T8FF test specimen and the results of the numerical analysis are given in Fig. 24. The peak force for T8FF test specimen occurs around 325 kN as in T4FF specimens (see Figs. 21 and 23). Figure 24 shows that T8FF multi-cell tubes start to deform from the lower end of the tube after the peak force is reached. Tearing is observed at the corners in both test specimens and the FEA model. Deformation behaviors of T4FF and T8FF are similar, and the tubes experience significant plastic deformation with cracks. The numerical models also successfully capture the splitting that occurs at the corners of the tube.

Since tube T8FF1 completely collapsed, the test was stopped for specimen 1 when the deformation distance reached 80 mm. Therefore, energy absorption parameters are calculated for 80 mm displacement for foam-filled T8 tubes as given in Table 6. The average SEA of T8FF specimens is calculated to be 14.592 kJ/kg, whereas the corresponding SEA value obtained through FEA is 16.906 kJ/kg, with a 15.86% error. The maximum error between the experimental and FEA results is in CFE value which is 17.24%.

Table 5 compares the crashworthiness results for multi-cell tubes T4FF, whereas Table 6 compares the results for multi-cell tubes T8FF. The results of the experiments and the FEA are in agreement.

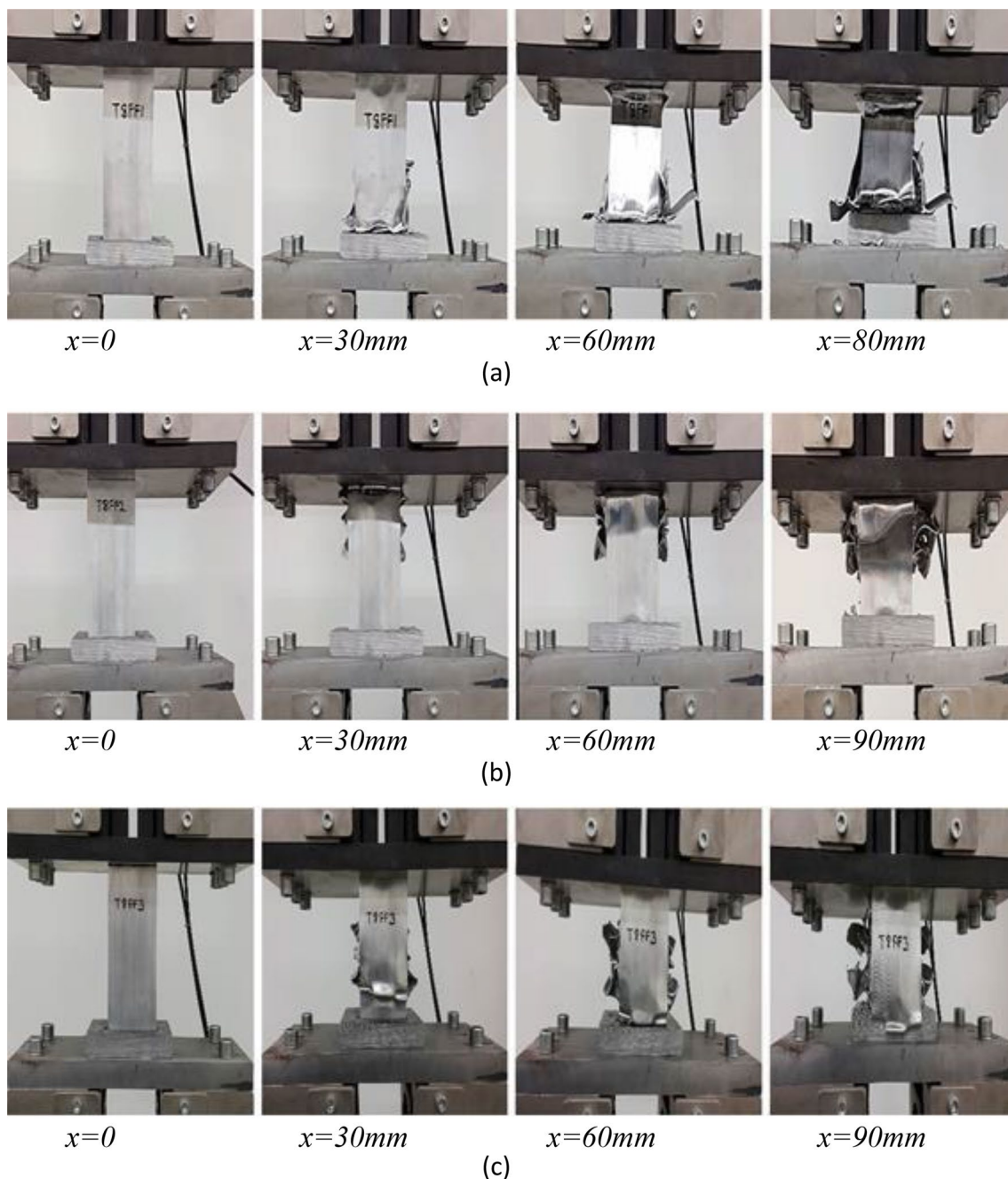


Fig. 15 Deformation views of multi-cell foam-filled T8FF specimens at different displacements: $x = 0$ mm, $x = 30$ mm, $x = 60$ mm, $x = 90$ mm
a T8FF1 **b** T8FF2 **c** T8FF3

5.2.3 Theoretical results for foam-filled T4FF and T8FF multi-cell tubes

For foam-filled tubes mean force is calculated using Eq. (10) where σ_f the foam plateau stress and c can be calculated using Eq. (9) where a and b are the cross-section of the rectangular foam.

P_{tube} was calculated 104.811 kN for empty multi-cell tube T4E. The mean force of T4FF tube can be calculated

from Eq. (10) as 204.8 MPa where $a = 68$ mm, $b = 82$ mm, $A_f = 5160.75$ mm², $t = 1.5$ mm and $\sigma_f = 12.8$ MPa, C_{avg} is a linear increasing function of deformation and equal to 5.5 [53].

P_{tube} was calculated 101.7 kN for empty multi-cell tube T8E and $A_f = 5160.75$ mm². Mean force of T8FF tube can be calculated from Eq. (10) as 208.7 MPa

The mean crush forces that the simulation and empirical formula estimated are shown in Table 7. The FE results

Fig. 16 Force-displacement graph of multi-cell foam-filled T8FF test specimens

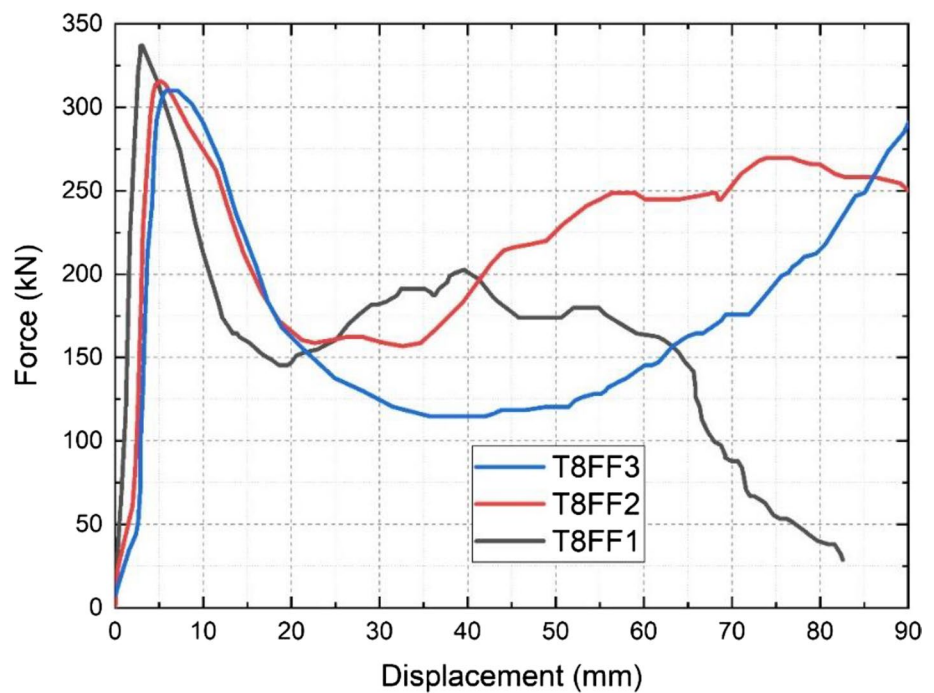
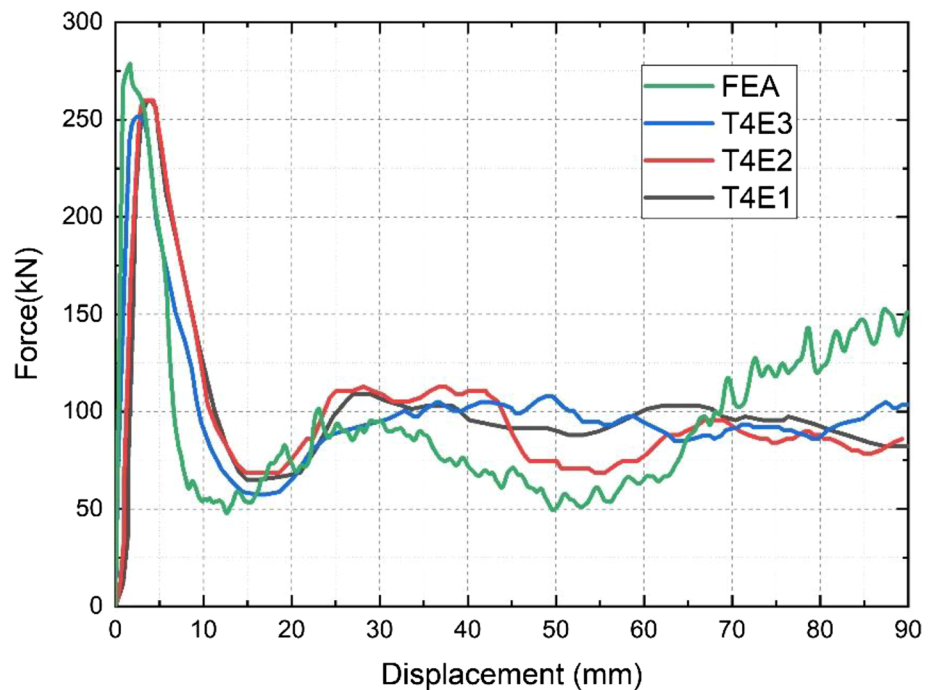


Fig. 17 Crushing force-displacement graphs for multi-cell empty T4E tubes



match the mean forces calculated using the empirical formula and the experimental data.

The mean force according to empirical formula is 204.8 kN, with a -13.0% error, as compared to the mean force obtained via tests, which is 241.4 kN for T4FF tubes. The mean force according to empirical formula is 208.69 kN for T8FF tubes, with a 11.73% error, as compared to the mean force obtained via tests, which is 186.8 kN for T8FF tubes.

The simulation values coincide with the mean forces derived from the empirical formula and experimental results.

5.3 Comparison and discussion of the results for empty and foam filled tubes

Table 8 presents the normalized crashworthiness metrics (CFE and SEA) for empty and foam filled tubes. According

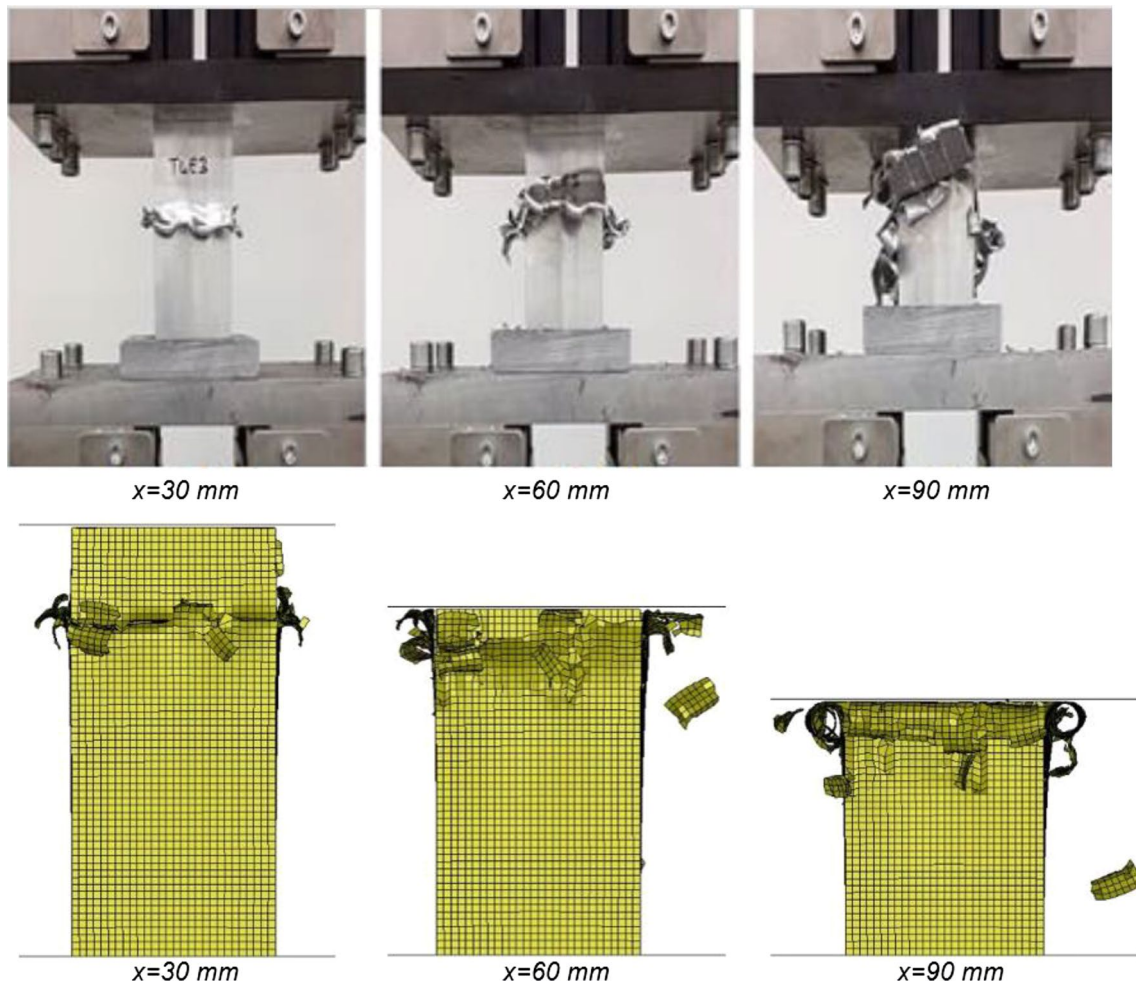
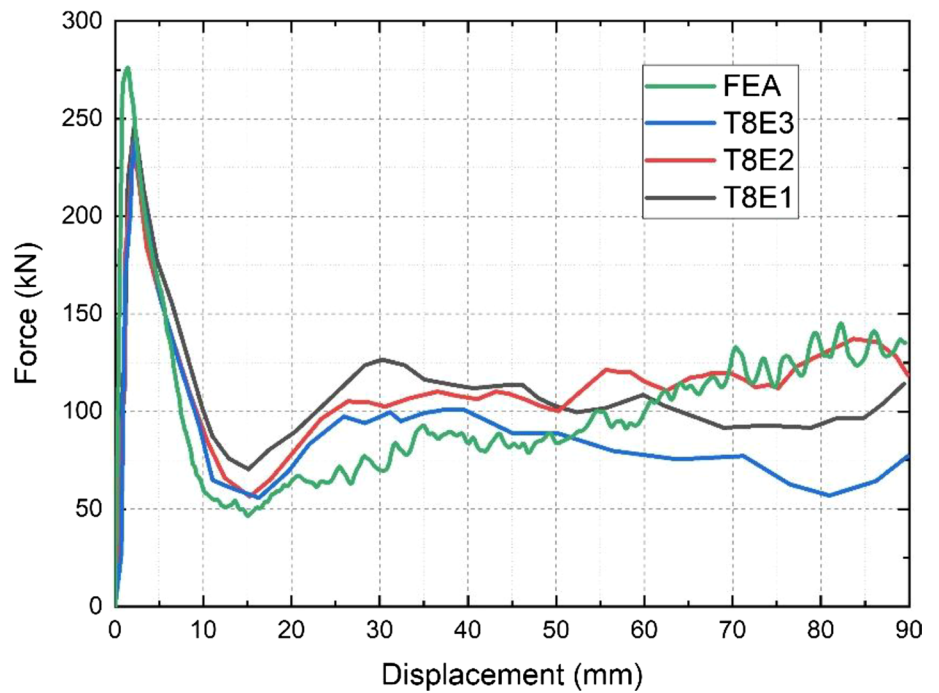


Fig. 18 Comparison of collapse modes of multi-cell empty T4E tubes between experimental and FEA result

Fig. 19 Crushing force-displacement graphs for multi-cell empty T8E tubes



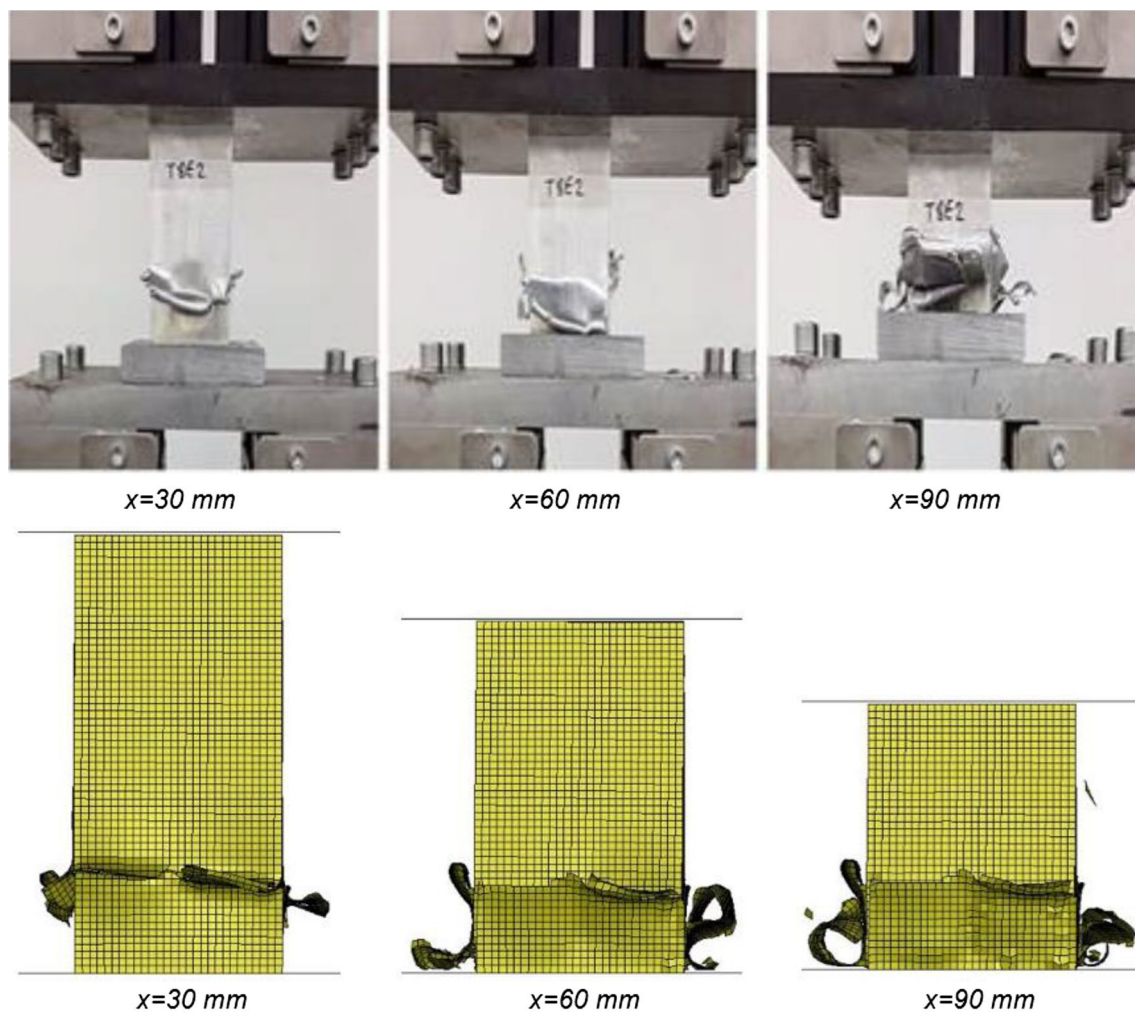


Fig. 20 Comparison of collapse modes of multi-cell empty T8E tubes between experimental and FEA results

to Table 8 T4FF has the largest CFE value (0.72) and T8E has the largest SEA value (21.51 kJ/kg). As a general conclusion, foam filled tubes have greater CFE than their empty counterparts. However this does not hold true for their SEA performance. For instance, T8FF displayed the worst SEA performance. It can be concluded that the use of Al foam is efficient in terms of reducing the maximum crash force thereby the CFE, however it is not efficient in terms of energy absorption performance per unit mass.

Since the number of T shape, left corner, and criss-cross elements in multi-cell tubes varies in numbers, the force-displacement graphs and energy absorption metrics differ for tubes. According to Eq. (10), foam interaction has a significant effect on the mean crush force of multi-cell tubes. Due to the number of corner and criss-cross elements and foam interactions of multi-cell tubes, mean forces and absorbed energy differs significantly for T4FF and T8FF tubes. Although the masses are similar for

foam-filled tubes, T4FF model has higher mean force and SEA due to better foam interaction.

A load drop after peak force in catastrophic failure of T8FF tubes resulted in lower SEA due to the ruptured tube corners and overflow of the foam. After the first load drop of T8FF tubes, the crushing force does not increase much as the tube deforms as compared to T4FF tubes. Therefore T8FF tubes displayed the worst SEA performance among all the tubes considered in this study.

6 Conclusions

This study used experimental, numerical, and theoretical analyses to examine the crashworthiness of multi-cell empty and foam filled aluminum tubes under axial compression. Information on deformation patterns and failure mechanisms for each stage of the crushing process is valuable and can be found using a validated finite element model. Figure 25

Fig. 21 Crushing force-displacement graphs for multi-cell foam-filled T4FF tubes

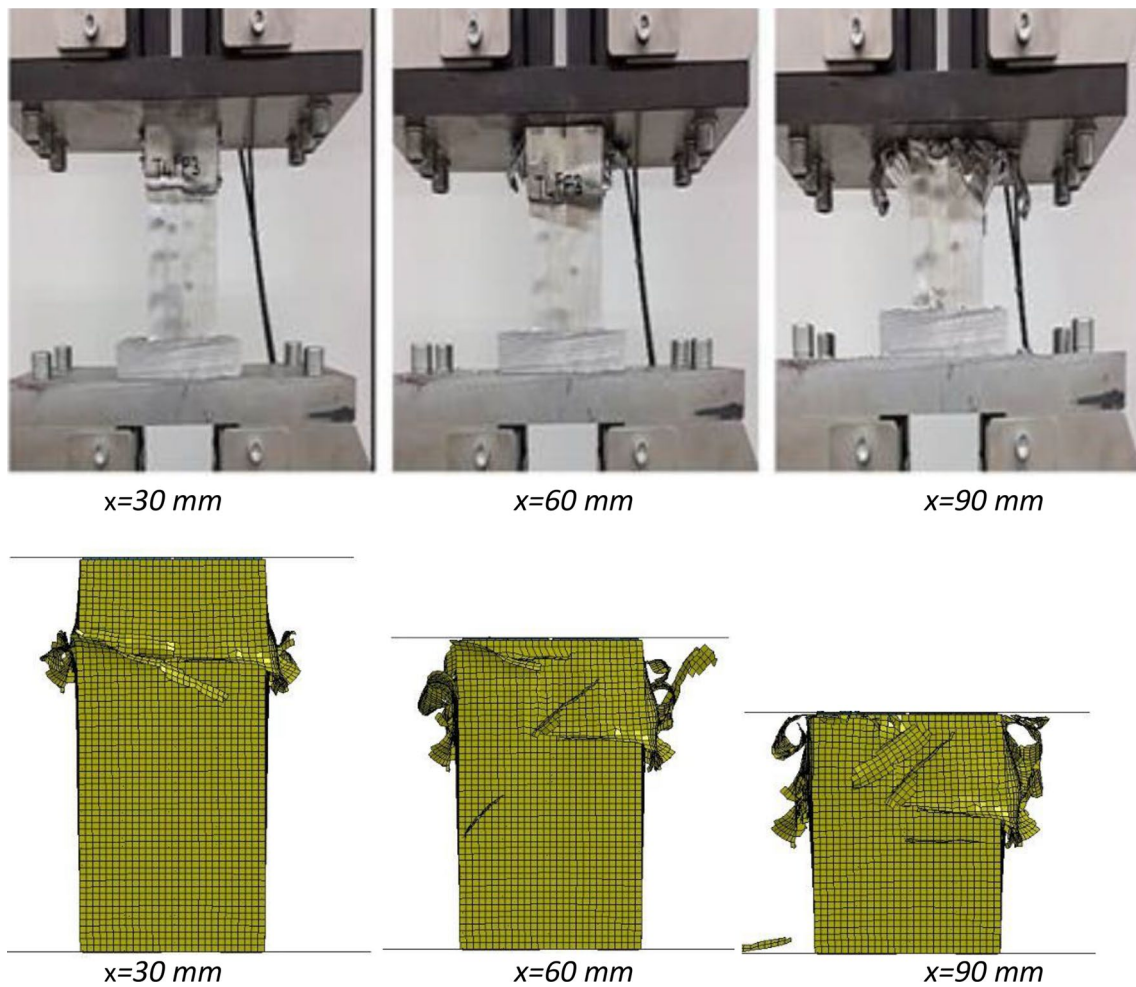
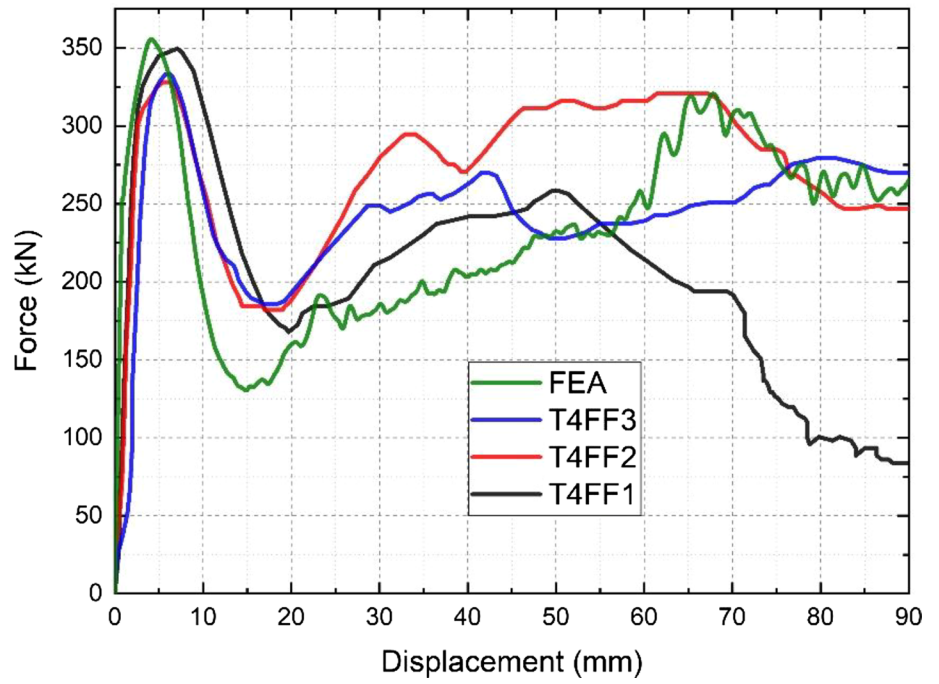
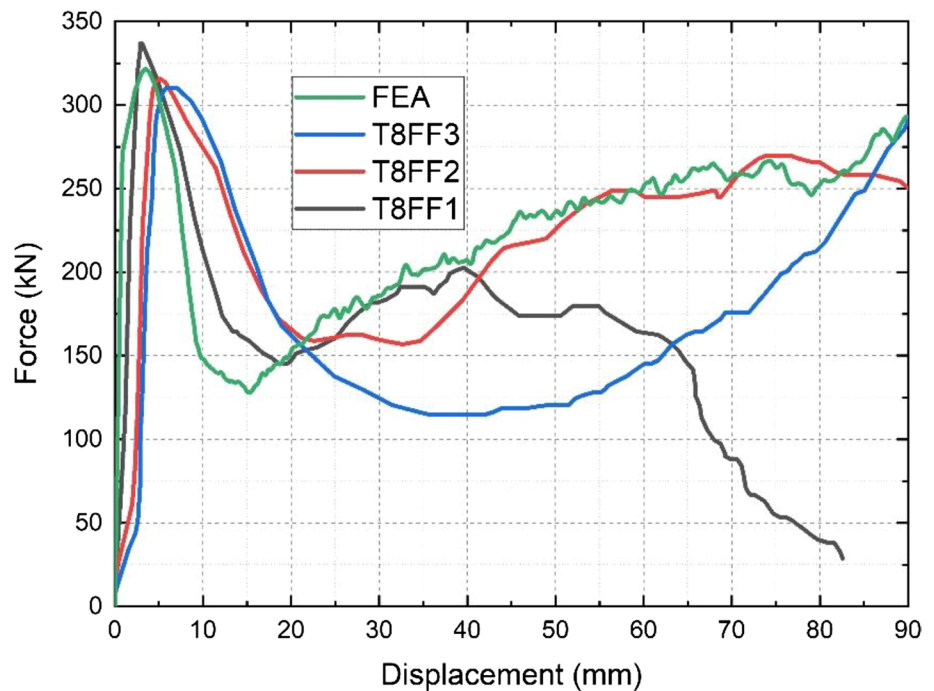


Fig. 22 Collapse modes of multi-cell foam filled T4FF tubes between experimental and FEA results

Fig. 23 Crushing force-displacement graphs for multi-cell foam-filled T8FF tubes



shows a comparison of the deformation patterns for empty multi-cell tubes at 30 mm, 60 mm, and 90 mm, and Fig. 26 shows the deformation patterns for foam filled multi-cell tubes at 30 mm, 60 mm, and 90 mm. The crashworthiness performance of the tubes was evaluated by using EA, SEA, IPCF, MCF, and CFE as well as deformation views of the tubes. From the results obtained, the following conclusions were reached:

- The MCF predictions obtained through the theoretical analysis agreed well with the ones obtained from experiments and FEA.
- The theoretical analysis predicted the MCF of empty multi-cell tubes with an error percentage less than 5%. Additionally, the theoretical analysis determined the MCF of foam-filled multi-cell tubes with an error percentage less than 13%.
- The IPCF values of the T8E and T8FF tubes were smaller than those of the T4E and T4FF tubes, respectively.
- The CFE, EA, and SEA of the T8E tubes were greater than those of the T4E tubes.
- The SEA and CFE of T8E tubes were 5.69% and 10.26% higher than those of the T4E tubes, respectively.
- Aluminum foam inside the T4 multi-cell tube (T4FF) improves the EA and CFE by 140.77% and 84%, respectively, but does not improve the SEA.

- Foam-filled multi-cell tubes showed noticeably better performance than empty multi-cell tubes in terms of CFE and EA.
- The SEA and CFE of T4FF tubes were 39.39% and 24.14% higher than those of the T8FF tubes, respectively.
- The T4FF tubes were the most crashworthy. The highest amount of SEA and CFE values were observed for T4FF tubes.
- The failure mechanisms for the crushing process of the tubes were similar. The cracks on the tubes cause the tubes to rupture and fail catastrophically after the deformation initiated at the middle of the tube height.

The material model used in the FE model is essential for accurately simulating the crash tests of thin-walled aluminum multi-cell tubes. The FE model generates consistent energy absorption parameters with the experimental results by determining appropriate material model, contact mechanisms and boundary conditions. The mean force values of empty and foam-filled multi-cell tubes can be predicted using an empirical formula when the geometrical properties and foam characteristics are defined.

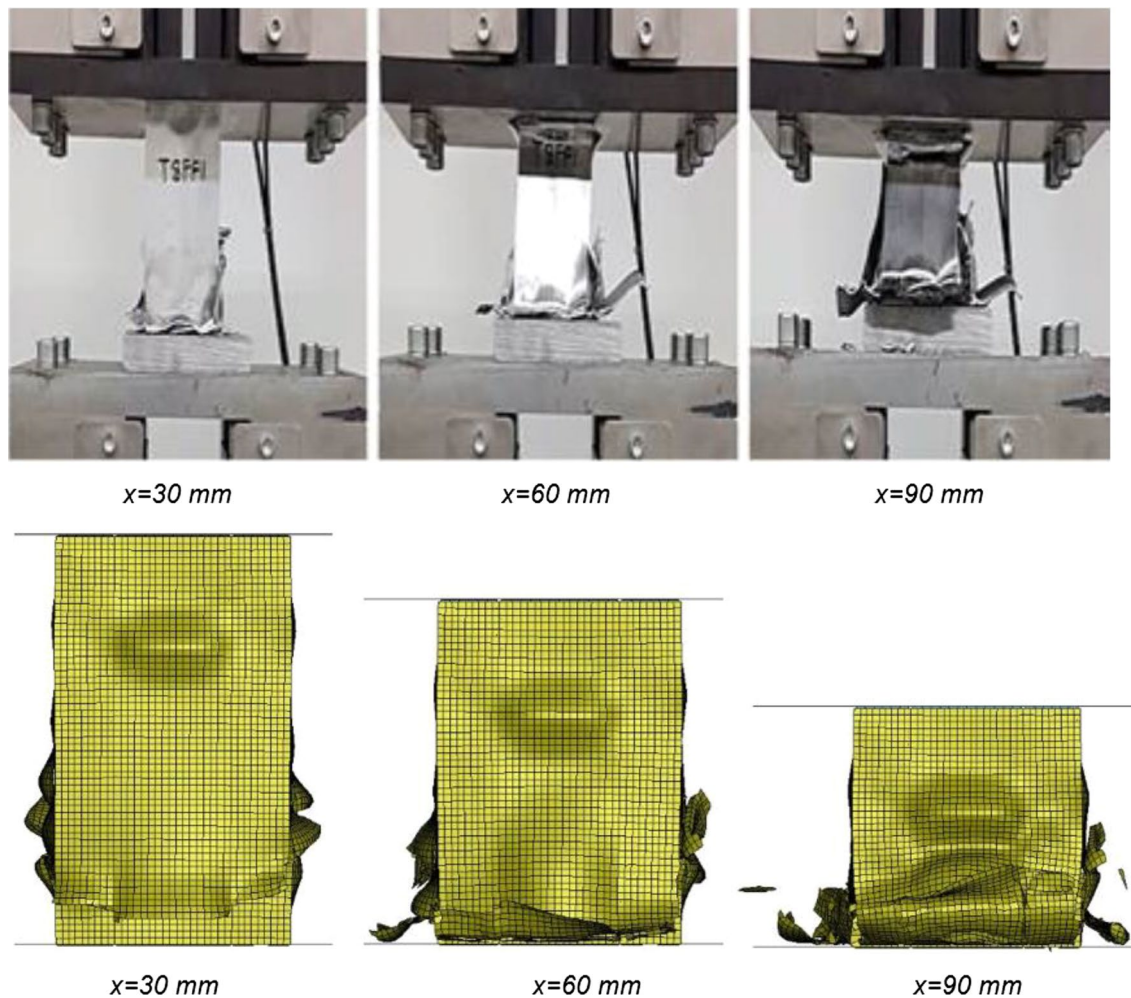


Fig. 24 Comparison of collapse modes of multi-cell foam-filled T8FF tubes between experimental and FEA results

Appendix

A crashworthiness metrics used in energy absorber design

The tube geometry, length, and wall thickness of tubes are the three main tube dimensions that researchers are most interested in. Based on the determined failure modes and measured crashworthiness measures, the impact of geometry and material properties is studied. Numerous methods were researched to increase the efficiency of the crush force while decreasing the initial peak force to absorb more energy.

Based on the determined failure modes and measured crashworthiness measures, the impact of geometry and material properties is studied. These measurements include

total energy absorption (EA), specific energy absorption (SEA), initial peak force, mean force, and crush force efficiency (CFE).

A.1 Total energy absorption (EA)

EA is calculated by determining the area under the force-displacement curve. Consequently, The formula below can be used to determine EA as:

$$EA = \int_0^{x_c} F dx \quad (19)$$

where F is the crushing force, and x_c is the cut-off displacement.

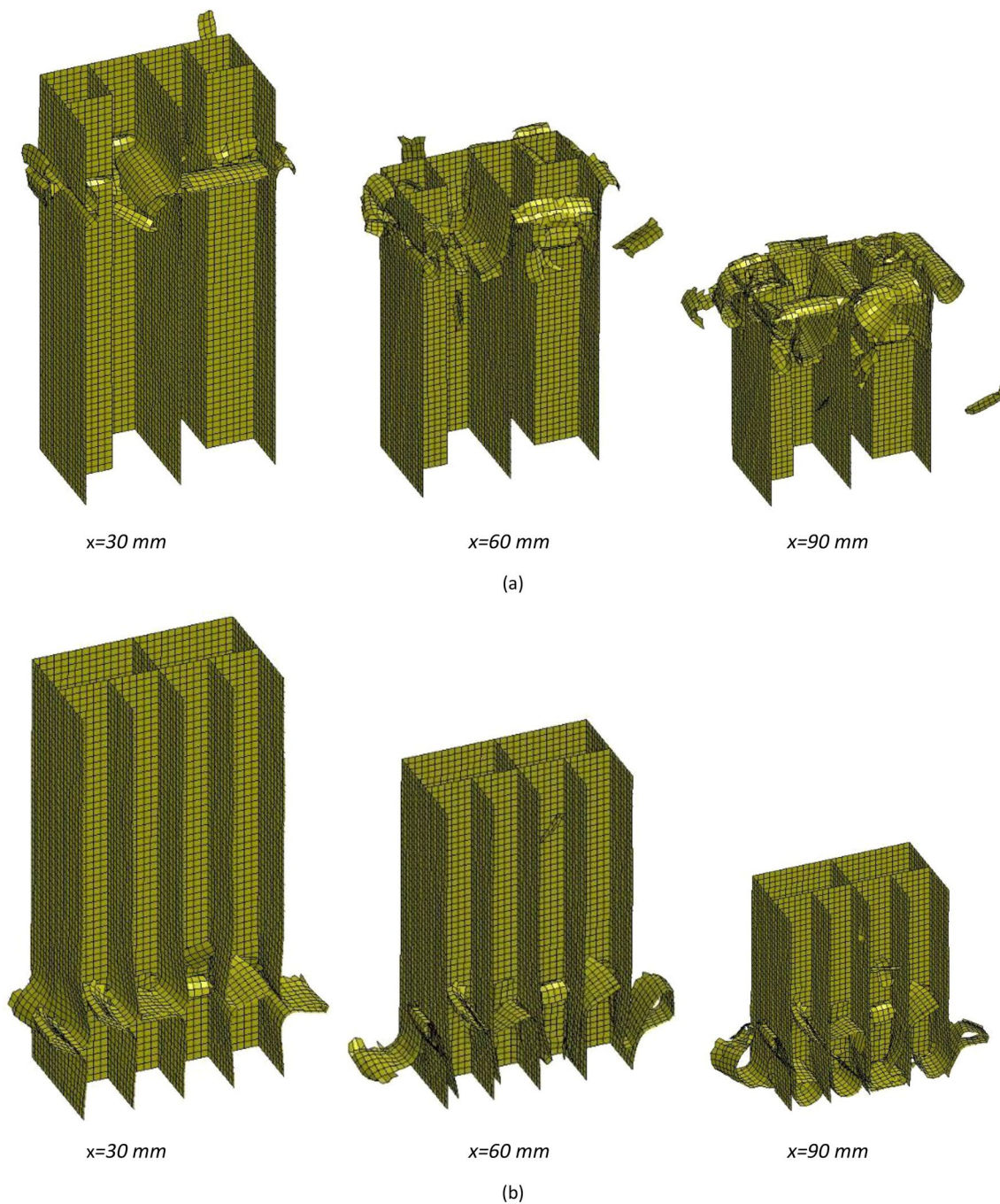


Fig. 25 Deformed views at 30 mm, 60 mm, and 90 mm of deformation of multi-cell empty tubes: **a** T4E tubes **b** T8E tubes

A.2 Specific energy absorption (SEA)

For energy absorbers, the amount of energy absorbed per unit of mass is crucial. One way to express the Specific Energy Absorption (*SEA*) is as follows:

$$SEA = \frac{\text{Total Energy Absorbed}}{\text{Total Mass}} = \frac{EA}{m} \quad (20)$$

where m is the mass of the structure.

A.3 Initial peak crush force (IPCF)

The first peak is identified for the initial peak crush force of the force-displacement graph.

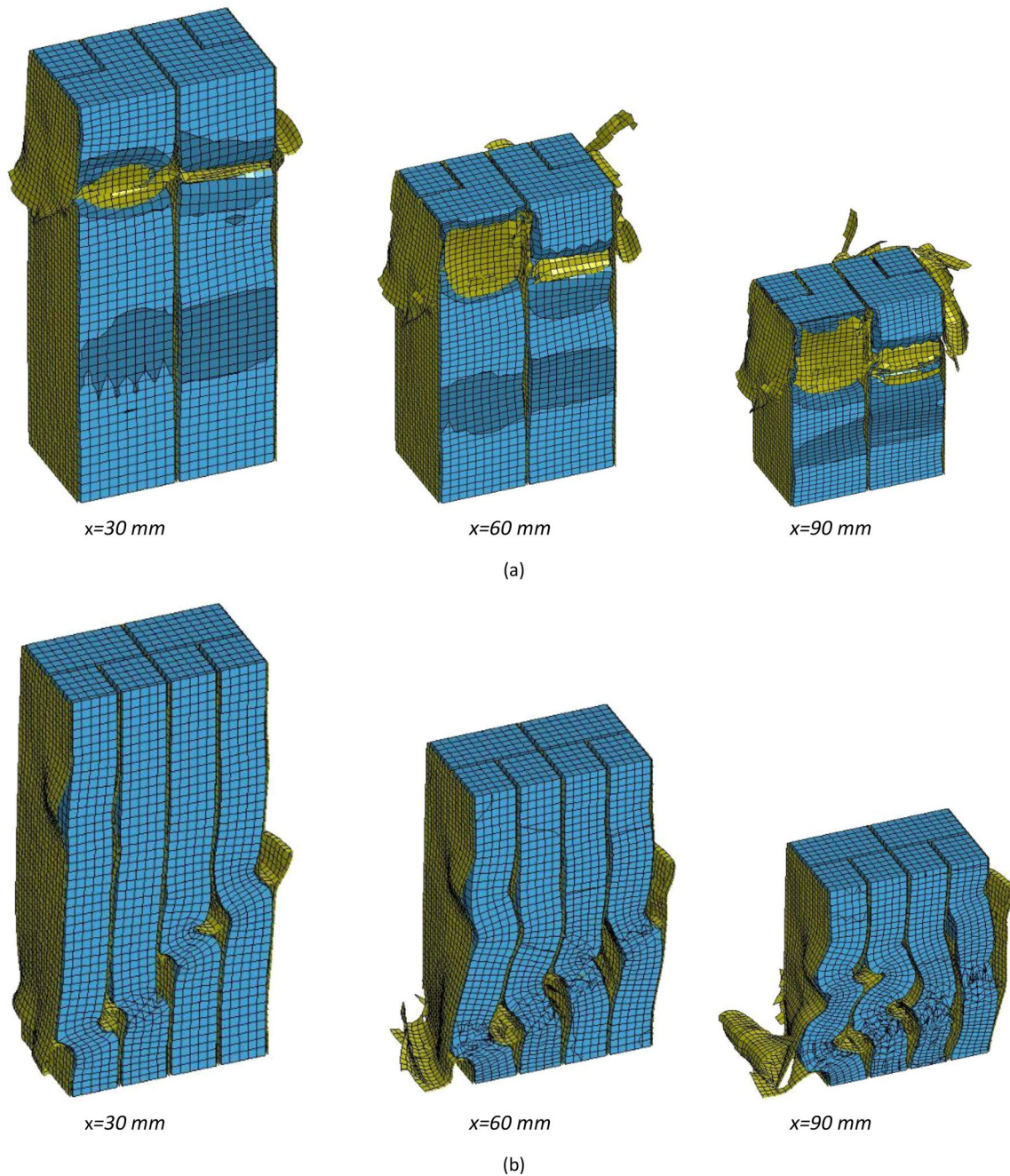


Fig. 26 Deformed views at 30 mm, 60 mm, and 90 mm of deformation of multi-cell foam-filled tubes: **a** T4FF tubes **b** T8FF tubes

A.4 Mean crush force (MCF)

The ratio of the EA to the cut-off deformation, x_c , determines the mean crush force, MCF which can be expressed by the following equation:

$$MCF = \frac{EA}{x_c} \tag{21}$$

A.5 Crush force efficiency (CFE)

The ratio of MCF to $IPCF$ is known as the CFE which can be expressed as:

$$CFE = \frac{MCF}{IPCF} \tag{22}$$

The ultimate objective of an energy absorber design is to get high *SEA*, *MCF* and *CFE* but small *IPCF* values.

Acknowledgements The experimental results obtained in this paper is from the research project which was supported by TUBITAK (the Scientific and Technological Research Council of Türkiye) under the ARDEB-1002 Program (Project Number 115M025).

Declarations

Conflict of interest The authors declare that they have no conflict of interest.

References

- Nia AA, Parsapour M (2014) Comparative analysis of energy absorption capacity of simple and multi-cell thin-walled tubes with triangular, square, hexagonal and octagonal sections. *Thin-Walled Struct* 74:155–165
- Fang J, Gao Y, Sun G, Qiu N, Li Q (2015) On design of multi-cell tubes under axial and oblique impact loads. *Thin-Walled Struct* 95:115–126
- Tang Z, Liu S, Zhang Z (2013) Analysis of energy absorption characteristics of cylindrical multi-cell columns. *Thin-Walled Struct* 62:75–84
- Zhang X, Zhang H (2014) Axial crushing of circular multi-cell columns. *Int J Impact Eng* 65:110–125
- Yang F, Deng X (2023) Study on the crashworthiness of star-shaped multicellular tubes. *Mech Adv Mater Struct*, 1–18
- Koloushani M, Forouzan MR, Niroomand MR (2023) On the crashworthiness performance of thin-walled circular tubes: Effect of diameter and thickness. *Mech Adv Mater Struct*, 1–13
- Ma X, Tian X (2022) Crushing behaviour of a novel hybrid multi-cell structure. *J Braz Soc Mech Sci Eng* 44(9):383
- Albak Eİ, Solmaz E, Yıldız AR, Öztürk F (2021) Multiobjective crashworthiness optimization of graphene type multi-cell tubes under various loading conditions. *J Braz Soc Mech Sci Eng* 43(5):266
- Akhavan Attar A, Rasouli S, Chahardoli S (2020) Effect of combined multi-cell columns and exterior stiffeners on energy absorption parameters of thin-walled tubes under axial load. *J Braz Soc Mech Sci Eng* 42:1–16
- Wu S, Zheng G, Sun G, Liu Q, Li G, Li Q (2016) On design of multi-cell thin-wall structures for crashworthiness. *Int J Impact Eng* 88:102–117
- Chen T, Zhang Y, Lin J, Lu Y (2019) Theoretical analysis and crashworthiness optimization of hybrid multi-cell structures. *Thin-Walled Struct* 142:116–131
- Gao Q, Wang L, Wang Y, Wang C (2016) Crushing analysis and multiobjective crashworthiness optimization of foam-filled ellipse tubes under oblique impact loading. *Thin-Walled Struct* 100:105–112
- Kılıçaslan C (2015) Numerical crushing analysis of aluminum foam-filled corrugated single-and double-circular tubes subjected to axial impact loading. *Thin-Walled Struct* 96:82–94
- Qi C, Yang S (2014) Crashworthiness and lightweight optimisation of thin-walled conical tubes subjected to an oblique impact. *Int J Crashworthiness* 19(4):334–351
- Ahmad Z, Thambiratnam D (2009) Crushing response of foam-filled conical tubes under quasi-static axial loading. *Mater Des* 30(7):2393–2403
- Toksoy AK, Güden M (2011) The optimisation of the energy absorption of partially al foam-filled commercial 1050h14 and 6061t4 al crash boxes. *Int J Crashworthiness* 16(1):97–109
- Altin M, Güler MA, Mert SK (2017) The effect of percent foam fill ratio on the energy absorption capacity of axially compressed thin-walled multi-cell square and circular tubes. *Int J Mech Sci* 131:368–379
- Nikkhah H, Guo F, Chew Y, Bai J, Song J, Wang P (2017) The effect of different shapes of holes on the crushing characteristics of aluminum square windowed tubes under dynamic axial loading. *Thin-Walled Struct* 119:412–420
- Zhang X, Cheng G (2007) A comparative study of energy absorption characteristics of foam-filled and multi-cell square columns. *Int J Impact Eng* 34(11):1739–1752
- Li Z, Ma W, Hou L, Xu P, Yao S (2020) Crashworthiness analysis of corrugations reinforced multi-cell square tubes. *Thin-Walled Struct* 150:106708
- Reyes A, Langseth M, Hopperstad OS (2003) Square aluminum tubes subjected to oblique loading. *Int J Impact Eng* 28(10):1077–1106
- Qiao J, Chen J, Che H (2006) Crashworthiness assessment of square aluminum extrusions considering the damage evolution. *Thin-walled struct* 44(6):692–700
- Marzbanrad J, Keshavarzi A, Aboutalebi FH (2014) Influence of elastic and plastic support on the energy absorption of the extruded aluminium tube using ductile failure criterion. *Int J Crashworthiness* 19(2):172–181
- Allahbakhsh H, Saemi J, Hourali M (2011) Design optimization of square aluminium damage columns with crashworthiness criteria. *Mechanics* 17(2):187–192
- Estrada Q, Szwedowicz D, Silva-Aceves J, Majewski T, Vergara-Vazquez J, Rodríguez-Mendez A (2017) Crashworthiness behavior of aluminum profiles with holes considering damage criteria and damage evolution. *Int J Mech Sci* 131:776–791
- Estrada Q, Szwedowicz D, Rodríguez-Mendez A, Gómez-Vargas OA, Elias-Espinosa M, Silva-Aceves J (2018) Energy absorption performance of concentric and multi-cell profiles involving damage evolution criteria. *Thin-Walled Struct* 124:218–234
- Hooputra H, Gese H, Dell H, Werner H (2004) A comprehensive failure model for crashworthiness simulation of aluminium extrusions. *Int J Crashworthiness* 9(5):449–464
- Estrada Q, Szwedowicz D, Baltazar M, Cortes C, Majewski T, Estrada CA (2016) The performance of energy absorption in structural profiles with different discontinuities. *Int J Adv Manuf Technol* 84(5–8):1081–1094
- Mert SK, Demiral M, Altin M, Acar E, Güler MA (2021) Experimental and numerical investigation on the crashworthiness optimization of thin-walled aluminum tubes considering damage criteria. *J Braz Soc Mech Sci Eng* 43:1–22
- Goel MD (2015) Deformation, energy absorption and crushing behavior of single-, double-and multi-wall foam filled square and circular tubes. *Thin-walled struct* 90:1–11
- Hanssen A, Hopperstad OS, Langseth M, Ilstad H (2002) Validation of constitutive models applicable to aluminium foams. *Int J Mech Sci* 44(2):359–406
- Deshpande VS, Fleck NA (2000) Isotropic constitutive models for metallic foams. *J Mech Phys Solids* 48(6–7):1253–1283
- Reyes A, Hopperstad O, Berstad T, Langseth M (2004) Implementation of a constitutive model for aluminum foam including fracture and statistical variation of density. In: *Proceedings of 8th International LS-DYNA Users Conference*, pp 11–24
- Yin H, Wen G, Liu Z, Qing Q (2014) Crashworthiness optimization design for foam-filled multi-cell thin-walled structures. *Thin-Walled Struct* 75:8–17

35. Zhang Y, Ge P, Lu M, Lai X (2018) Crashworthiness study for multi-cell composite filling structures. *Int J Crashworthiness* 23(1):32–46
36. Sun G, Liu T, Huang X, Zheng G, Li Q (2018) Topological configuration analysis and design for foam filled multi-cell tubes. *Eng Struct* 155:235–250
37. Alexander JM (1960) An approximate analysis of the collapse of thin cylindrical shells under axial loading. *Q J Mech Appl Math* 13(1):10–15
38. Wierzbicki T, Abramowicz W (1983) On the crushing mechanics of thin-walled structures. *J Appl Mech* 50:727–734,12
39. Abramowicz W, Wierzbicki T (1989) Axial crushing of multi-corner sheet metal columns. *J Appl Mech* 56:113–120,03
40. Abramowicz W, Jones N (1984) Dynamic axial crushing of square tubes. *Int J Impact Eng* 2(2):179–208
41. Abramowicz W, Jones N (1986) Dynamic progressive buckling of circular and square tubes. *Int J Impact Eng* 4(4):243–270
42. Andrews K, England G, Ghani E (1983) Classification of the axial collapse of cylindrical tubes under quasi-static loading. *Int J Mech Sci* 25(9–10):687–696
43. Santosa S, Wierzbicki T (1998) Crash behavior of box columns filled with aluminum honeycomb or foam. *Comput Struct* 68(4):343–367
44. Hanssen AG, Langseth M, Hopperstad OS (2000) Static and dynamic crushing of circular aluminium extrusions with aluminium foam filler. *Int J Impact Eng* 24(5):475–507
45. Santosa SP, Wierzbicki T, Hanssen AG, Langseth M (2000) Experimental and numerical studies of foam-filled sections. *Int J Impact Eng* 24(5):509–534
46. Chen W, Wierzbicki T (2001) Relative merits of single-cell, multi-cell and foam-filled thin-walled structures in energy absorption. *Thin-Walled Struct* 39(4):287–306
47. Niknejad A, Liaghat G, Naeni HM, Behraves A (2011) Theoretical and experimental studies of the instantaneous folding force of the polyurethane foam-filled square honeycombs. *Mater Des* 32(1):69–75
48. Niknejad A, Abedi M, Liaghat G, Nejad MZ (2015) Absorbed energy by foam-filled quadrangle tubes during the crushing process by considering the interaction effects. *Arch Civil Mech Eng* 15(2):376–391
49. Abedi MM, Niknejad A, Liaghat GH, Nejad MZ (2012) Theoretical and experimental study on empty and foam-filled columns with square and rectangular cross section under axial compression. *Int J Mech Sci* 65(1):134–146
50. Sun G, Pang T, Xu C, Zheng G, Song J (2017) Energy absorption mechanics for variable thickness thin-walled structures. *Thin-Walled Struct* 118:214–228
51. Xie S, Yang W, Wang N, Li H (2017) Crashworthiness analysis of multi-cell square tubes under axial loads. *Int J Mech Sci* 121:106–118
52. Zhang X, Cheng G, Zhang H (2006) Theoretical prediction and numerical simulation of multi-cell square thin-walled structures. *Thin-Walled Struct* 44(11):1185–1191
53. Googarchin HS, Pasandidehpour M, Mahmoodi A, Shojaeefard M (2019) Energy absorption analysis for tapered multi-cell tubes improved by foams: theoretical development and numerical simulation. *Compos Struct* 207:213–222
54. Acar E, Altin M, Güler MA (2019) Evaluation of various multi-cell design concepts for crashworthiness design of thin-walled aluminum tubes. *Thin-Walled Struct* 142:227–235
55. Ls-Dyna L-D (2016) Keyword users manual-volume ii: Material models. Livermore Software Technology Corporation, Livermore
56. Rathnaweera G, Ruan D, Hajj M, Durandet Y (2014) Performance of aluminium/terocore® hybrid structures in quasi-static three-point bending: experimental and finite element analysis study. *Mater Des* 1980–2015(54):880–892
57. Bilston D, Rathnaweera G, Ruan D, Hajj M, Durandet Y (2016) Parametric study of the bending properties of lightweight tubular metal/polymer foam hybrid structures. *Compos B Eng* 105:101–110
58. Yu Z, Amdahl J (2016) Full six degrees of freedom coupled dynamic simulation of ship collision and grounding accidents. *Mar Struct* 47:1–22
59. Shi S, Lam N, Cui Y, Zhang L, Lu G, Gad E (2022) Indentation into an aluminium panel by the impact of a rigid spherical object. *Thin-Walled Struct* 180:109935
60. Harral A (2022) Material properties of aluminum 6061 t6 for mat_18,” 2018. <https://varmintal.com> Accessed 07 Dec 2022
61. Altin M, Acar E, Güler M (2018) Foam filling options for crashworthiness optimization of thin-walled multi-tubular circular columns. *Thin-Walled Struct* 131:309–323
62. Güler MA, Cerit ME, Mert SK, Acar E (2020) Experimental and numerical study on the crashworthiness evaluation of an intercity coach under frontal impact conditions. *Proc Inst Mech Eng Part D J Automob Eng* 234(13):3026–3041
63. Leclerc P, Toussaint G (2018) Constitutive models investigation to simulate damage/failure of aluminium (al) 6061-t6. tech. rep., Defence Research and Development Canada
64. Arcillas A (2022) Mechanical behavior, testing, and manufacturing properties of materials. <https://www.academia.edu/25452539> Accessed on 07 Dec 2022

Publisher's Note Springer Nature remains neutral with regard to jurisdictional claims in published maps and institutional affiliations.

Springer Nature or its licensor (e.g. a society or other partner) holds exclusive rights to this article under a publishing agreement with the author(s) or other rightsholder(s); author self-archiving of the accepted manuscript version of this article is solely governed by the terms of such publishing agreement and applicable law.